Paleoceanography and Paleoclimatology

RESEARCH ARTICLE
10.1029/2019PA003823

Carbon Export Buffering and CO_2 Drawdown by Flexible Phytoplankton C:N:P Under Glacial Conditions

Katsumi Matsumoto[1], Rosalind Rickaby[2], and Tatsuro Tanioka[1]

[1]Department of Earth and Environmental Sciences, University of Minnesota, Minneapolis, MN, USA, [2]Department of Earth Sciences, University of Oxford, Oxford, UK

Key Points:
- Local organic matter C:N:P is controlled by phytoplankton community composition and physiology
- Global export C:N:P is strongly increased by regional production changes through sea ice expansion under glacial conditions
- Allowing flexible C:N:P under glacial conditions strongly buffers POC export and reduces atmosphere pCO_2 by ~20 μatm

Supporting Information:
- Supporting Information S1

Correspondence to:
K. Matsumoto,
katsumi@umn.edu

Citation:
Matsumoto, K., Rickaby, R., & Tanioka, T. (2020). Carbon export buffering and CO_2 drawdown by flexible phytoplankton C:N:P under glacial conditions. *Paleoceanography and Paleoclimatology*, *35*, e2019PA003823. https://doi.org/10.1029/2019PA003823

Received 22 NOV 2019
Accepted 24 APR 2020
Accepted article online 9 MAY 2020

Abstract Modern observations indicate that variations in marine phytoplankton stoichiometry correlate with the boundaries of major surface waters. For example, phytoplankton in the oligotrophic subtropical gyres typically have much higher C:N:P ratios (i.e., higher C:P and higher N:P ratios) than those in eutrophic upwelling regions and polar regions. Such a spatial pattern points to nutrient availability as a key environmental driver of stochiometric flexibility. Environmental dependence of phytoplankton C:N:P opens unexplored possibilities for modifying the strength of the biological pump under different climate conditions. Here we present a power law formulation of C:N:P flexibility that is driven by nutrients, temperature, and light. We embed the formulation in a global ocean carbon cycle model with multiple phytoplankton types and explore biogeochemical implications under glacial conditions. We find three key controls on export C:N:P ratio: phytoplankton physiology and community structure as well as the balance in regional production at the global level. Glacial inputs of iron and sea ice expansion are important modifiers of these three controls. We also find that global export C:N:P increases substantially under glacial conditions, and this strongly buffers global carbon export against decrease and draws down approximately 20 μatm of atmospheric CO_2. These results point to the importance of including phytoplankton C:N:P flexibility in a mix of mechanisms that drive atmospheric CO_2 over glacial-interglacial time scale. Finally, our simulations indicate decoupling of nutrients, which may provide a resolution to the longstanding disagreement regarding nutrient utilization in the glacial Southern Ocean derived from different nutrient proxies.

1. Introduction

The biological pump of the ocean is one of the key drivers of the global carbon cycle (Volk & Hoffert, 1985). It is also known as the organic carbon pump or soft tissue pump. The pump refers to the sinking of particulate organic matter (POM) through the ocean water column that transports carbon from the surface ocean to remineralize in the ocean interior. The surface ocean interacts with the atmosphere, so carbon transported to the interior can be sequestered from the atmosphere for centuries until overturning circulation brings it back to the surface. In a series of publications, Broecker first introduced a number of ideas for how the biological pump could have been enhanced during the glacial period so as to lower atmospheric pCO_2 (Broecker, 1982a, 1982b; Broecker & Peng, 1982). Measurements from Antarctic ice cores demonstrate that pCO_2 was lower during peak glacial times by 80–100 μatm compared to interglacial periods (Barnola et al., 1987; Lüthi et al., 2008; Petit et al., 1999).

One well-known theme that emerged from Broecker's ideas called on increasing the oceanic inventories of nutrients that limit biological production in many parts of the world ocean today. The inventory of macronutrient phosphate (P) could have increased in response to the exposure and weathering of continental shelf sediments (Broecker, 1982a, 1982b). The inventory of nitrogen (N) could have increased if denitrification decreased (Altabet et al., 1995; Ganeshram et al., 1995) and/or if N_2 fixation increased (Falkowski, 1997), although a change in the whole ocean budget of a major nutrient sufficient to account for the entire CO_2 change would generate extensive deep ocean deoxygenation. The inventory of micronutrient iron (Fe) could have increased as the glacial dust deposition increased (Martin, 1990).

In the case of increasing the N inventory, the average N:P ratio of organic matter would have had to increase over the widely assumed N:P ~ 16 in order for the biological pump to ramp up (Broecker & Henderson, 1998). If there were no change in the P inventory, the extra supply of N would not be fully utilized by phytoplankton (with assumed N:P~16), and the parts of the ocean that were originally N limited simply become P limited. The possibility that phytoplankton N:P increased was also contemplated later (Archer et al., 2000) and

invoked to account for contrasting nutrient histories in the glacial Southern Ocean (Elderfield & Rickaby, 2000) but not embraced. In the reciprocal case where P inventory increases, a change in phytoplankton stoichiometry is not required to enhance the biological pump. The reason is that diazotrophs or N fixers are expected to become more competitive and the oceanic N inventory should increase (Redfield, 1934).

A much less known idea introduced by Broecker, suggested originally by Peter Weyl, is that the carbon export per unit P export (C:P) may have increased during glacial time (Broecker, 1982a). Indeed, the biological pump would be strengthened and atmospheric pCO_2 reduced, if C:P increased, assuming no change in P export. Weyl speculated that preferential remineralization of P in organic matter through heterotrophy could raise the C:P ratio of sinking organic matter. Broecker apparently neither embraced the idea nor found evidence for it in the paleo record.

The notion that phytoplankton stoichiometry is stable globally originates from the seminal work by Redfield (1934) and is a central tenet of chemical oceanography. The canonical Redfield ratio of marine organic matter is C:N:P = 106:16:1, which was later extended to oxygen (O_2) with O_2:P = −150 (Anderson, 1995). Biologists have long known that phytoplankton stoichiometry was flexible in individual cells (e.g., Droop, 1974), and Redfield himself noted stoichiometric flexibility (Redfield et al., 1963). There is no obvious physiological reason why there should be a strict C:N:P ratio (Geider & La Roche, 2002). There is now evidence of substantial variability even on an ocean basin scale. In particular, Martiny et al. (2013) show a clear global pattern to the stoichiometry measured in phytoplankton and POM: The C:N:P ratio is 195:28:1 in the warm nutrient-poor subtropical gyres, 137:18:1 in the warm nutrient-rich upwelling zones, and 78:13:1 in the nutrient-rich polar regions. This variability is not fully understood, and a full discussion is beyond the scope of this study. However, nutrient availability is already clearly recognized as a driver (C. A. Garcia et al., 2018), and we discuss additional drivers in section 2.2.

The ocean carbon cycle modeling community is beginning to respond to this development. As exemplified by the Ocean Carbon Cycle Model Intercomparison Project (Najjar et al., 2007), the community has long used a fixed, remineralization ratio of O_2:C:N:P = −170:117:16:1 (Anderson & Sarmiento, 1994). There have been some studies that explored carbon impacts of different but still fixed C:P ratios using 3-D model (Heinze et al., 1991) and box models (Galbraith & Martiny, 2015; Weber & Deutsch, 2010). The state of the art CMIP5/6 models are mixed in terms of adopting a fully flexible C:N:P. In CMIP5 (Bopp et al., 2013), C:N:P ratio is fixed in the American model CESM/BEC, French model IPSL/PISCES, and German model MPI/HAMOCC models. The C:N ratio is fixed in the American model GFDL/TOPAZ and British model HadGCM/Diat-HadOCC. The Italian model CMCC/PELAGOS has a fully flexible C:N:P ratio (Vichi et al., 2007). In CMIP6 (Arora et al., 2019), CESM/MARBL has a flexible C:P ratio, GFDL/COBALT has a fully flexible C:N:P, and the Canadian CanESM5/CMOC has a fixed ratio. Outside CMIP, Daines et al. (2014) describe a dynamical C:N:P within a 3-D ocean model that builds on the algal growth model of Shuter (1979). Ward et al. (2018) present a size structured, cell quota model that allows for dynamic C:P. Elsewhere, the linear C:P model of Galbraith and Martiny (2015), discussed below, is implemented in a box model (Moreno et al., 2018) and 3-D model (Buchanan et al., 2019; Ödalen et al., 2020).

In our previous work, we presented a power law model of flexible phytoplankton stoichiometry (Tanioka & Matsumoto, 2017). We formulated and incorporated the sensitivity of phytoplankton C:P to changes in phosphate availability in an earth system model with two types of marine phytoplankton. With it, we investigated the stoichiometric buffer effect under a future warming scenario. The traditional view is that as warming enhances ocean stratification, nutrient supply becomes diminished, and thus, the biological pump of carbon weakens. This view assumes a fixed C:P ratio. With a dynamic C:P however, a reduction in P supply is expected to increase phytoplankton C:P, so that even with a reduced supply of nutrients, particulate organic carbon (POC) export may not diminish. In other words, changes in phytoplankton C:N:P in response to nutrient availability can buffer carbon export from changing. The main aim of this study is to understand how this stoichiometric buffer effect may alter under glacial conditions in a global ocean model. Ödalen et al. (2020) use a similar global model and have the same aim as this study, but there are critical differences in how stoichiometry is represented in the two studies. The model of Ödalen et al. (2020) has a single phytoplankton type, whose P:C is a linear function of phosphate only. In this study, there are three phytoplankton types, each with a unique nonlinear C:N:P response to a fuller set of environmental drivers. These model

features allow us to effectively interrogate the stoichiometric effects of phytoplankton physiology and community composition under glacial conditions.

2. Models and Experiments

The starting point of all our model runs is a long (10^4 years), steady state simulation of the global model under preindustrial climate conditions. All sensitivity experiments, including the Control run, start from the equilibrium state and last 5,000 years.

2.1. Global Model

This study employs MESMO2, an Earth system model of intermediate complexity described elsewhere in detail (Matsumoto et al., 2008, 2013). The model components used here are a 3-D model of the global ocean physics and biogeochemistry, a 2-D energy-moisture balanced model of the atmosphere, and a 2-D thermodynamic and dynamic model of sea ice. The model components representing land biosphere and deep sea sedimentation are excluded in this study. Carbonate compensation is thus not simulated here. MESMO has been used previously in a number of process studies of the global distributions of carbon and carbon isotopes under conditions of the past, present, and future (Lee et al., 2011; Matsumoto et al., 2010; Matsumoto & Yokoyama, 2013; Sun & Matsumoto, 2010; Tanioka & Matsumoto, 2017; Ushie & Matsumoto, 2012) as well as in model intercomparison projects (Archer et al., 2009; Cao et al., 2009; Eby et al., 2013; Joos et al., 2013; Weaver et al., 2012; Zickfeld et al., 2013). MESMO2 has been calibrated against various ocean observations, including transient tracers (anthropogenic carbon, CFCs), deep ocean radiocarbon, as well as biogeochemical tracers (macronutrients, silicic acid).

MESMO has a coarse resolution, equal area grid with 10° increments in longitude and is uniform in sine of latitude. There are 16 vertical levels with the top two levels representing the surface 100 m, where biological production occurs. The coarse resolution makes MESMO computationally efficient, an important attribute for long paleo simulations. Ocean physics is updated 100 times per year (i.e., ~3.6 days/step) with a 5:1 gear ratio for ocean biogeochemistry (i.e., 20 time steps per year, ~18 days/step). Excessive mixing that arises in coarse resolution, z-coordinate grid is reduced by the Gent-McWilliams eddy mixing parameterizations (Griffies, 1998). The atmospheric model predicts surface air temperature and specific humidity as well as downwelling radiative forcing from atmospheric pCO_2. The sea ice model calculates ice cover, ice height, and ice temperature. In this study, the physical components of MESMO2 remain unchanged, while the ocean biogeochemical components have undergone modifications.

A number of modifications were made to the biogeochemistry model of MESMO for this study. The complete set of biogeochemical equations for this study is provided in the supporting information. The original ocean biogeochemistry model of MESMO2 calculated net primary production (NPP) by two phytoplankton functional types (PFTs), large and small, whose production depended on nutrients, light, temperature, and mixed layer depth (Matsumoto et al., 2013). We note that the model does not calculate the biomass of the PFTs per se. The large PFT represented fast growing, opportunistic diatoms, while the small PFT represented all other, smaller algae including coccolithophores.

In this study, we added diazotrophs as the third PFT, which necessitated a reorganization of PFTs. The three PFTs in this study are eukaryotes, cyanobacteria that do not fix N, and diazotrophs. As with the large PFT in MESMO2, an important trait of eukaryotes is that they grow fast in nutrient replete waters. This PFT thus represents larger algae such as diatoms with high maximum growth rate (V_{max}) and high half saturation constants (K_X, where X = nutrient). Coccolithophores are eukaryotes and are now represented by the same PFT (Figure S1). Thus, $CaCO_3$ production is linked to eukaryote production with a positive dependence on pH. In order to allow for $CaCO_3$ production without being tightly coupled to opal production within the same single PFT, we make use of the residual nitrate potential growth (RNPG) index (Balch et al., 2016). This index recasts the ambient nitrate and silicic acid concentrations into potential algal growth rates. The relative size of the silicic acid-dependent growth rate versus the nitrate-dependent growth rate, both calculated with the Michaelis-Menten formula, modifies the $CaCO_3$:organic C ratio. The RNPG index is useful under the low glacial atmospheric pCO_2, because without it, the high surface ocean pH would lead necessarily to a large $CaCO_3$ production even if the eukaryote production is fueled by silicic acid (i.e., diatoms).

The second PFT is non-N-fixing cyanobacteria that dominate the subtropical gyres. It represents *Prochlorococcus* and *Synechococcus*, which are slow growing but able to take up nutrients efficiently at low concentrations due to their small cell sizes. This PFT thus has distinctly lower V_{max} and K_X, and it is not limited by silicic acid.

The third PFT represents diazotrophs, which are able to fix atmospheric nitrogen gas as ammonia. *Trichodesmium* is a major group of diazotrophs and also cyanobacteria. However, in this study, *Trichodesmium* is part of the diazotroph PFT, and any reference to cyanobacteria hereafter will mean *Prochlorococcus* and *Synechococcus* and not *Trichodesmium*. Diazotrophs bear the higher energy cost of N_2 fixation, so they have a lower V_{max} than the other PFTs (Tyrrell, 1999). The efficiency at which diazotrophs carry out N_2 fixation is inversely related to the ambient nitrate concentration (Paulsen et al., 2017). We assume immediate release of fixed nitrogen as nitrate (Ilyina et al., 2013). Diazotrophs are limited only by phosphate and Fe. The introduction of diazotrophs allows for a dynamic N cycle in the ocean, whose long-term N inventory is controlled by the balance of N_2 fixation and denitrification. We implemented water column denitrification, which is set to occur in the model where dissolved O_2 concentration ($[O_2]$) falls below 22.5 μmol kg^{-1}, a threshold chosen to give the global denitrification rate of roughly 100 Tg-N $year^{-1}$. We treat denitrification in a similar approach to the GENIE model (Ridgwell et al., 2007), in which 2 moles of NO_3 are converted to 1 mole of N_2 and liberates 2.5 moles of O_2 as a byproduct. As we only have water column denitrification and not sedimentary denitrification, our model provides a first step in representing the full marine N cycle.

At any ocean grid cell, the contribution that any PFT makes to the community production (i.e., PFT fraction) is calculated as $NPP(i)/\sum NPP$, where $NPP(i)$ is the NPP in C of the PFT index i corresponding to eukaryotes, cyanobacteria, and diazotrophs, and $\sum NPP$ is the their sum. PFT fractions add to 1 and define the community composition.

As in the original MESMO2 biogeochemistry model, NPP in this model is split into POM and dissolved organic matter (DOM). Export production of POM, opal, and $CaCO_3$ is calculated at 100 m water depth without ballast effect. There is partial production under an incomplete coverage of sea ice. The rate of remineralization of sinking POM depends on temperature and sinking velocity. Nutrients that limit production are phosphate, nitrate, iron, and silicic acid. The limiting nutrient in each grid box is determined by the Liebig's rule of the minimum relative to the stoichiometry of uptake requirement, which in MESMO2 was fixed for C:N:P = 117:16:1 but variable for C:Fe and Si:N. Following observations (e.g., Franck et al., 2000; Sunda & Huntsman, 1995), both C:Fe and Si:N ratios increase as Fe concentration decreases. Iron is introduced into the model domain by aeolian deposition of dust at the surface following the modern flux pattern (Mahowald et al., 2006). Scavenging of free dissolved iron by sinking particles and binding of soluble iron to organic ligands facilitate iron cycling. Iron is removed from the model domain by iron-bearing particles reaching the sea floor, and this removal matches the aeolian input globally at steady state.

2.2. Power Law Model of Flexible Stoichiometry

In this study, the power law formulations of flexible P:C and N:C respectively take the form:

$$[P:C] = [P:C]_0 \cdot \left(\frac{[PO_4]}{[PO_4]_0}\right)^{s_{PO_4}^{P:C}} \cdot \left(\frac{[NO_3]}{[NO_3]_0}\right)^{s_{NO_3}^{P:C}} \cdot \left(\frac{T}{T_0}\right)^{s_T^{P:C}} \cdot \left(\frac{I}{I_0}\right)^{s_I^{P:C}}, \quad (1)$$

$$[N:C] = [N:C]_0 \cdot \left(\frac{[PO_4]}{[PO_4]_0}\right)^{s_{PO_4}^{N:C}} \cdot \left(\frac{[NO_3]}{[NO_3]_0}\right)^{s_{NO_3}^{N:C}} \cdot \left(\frac{T}{T_0}\right)^{s_T^{N:C}} \cdot \left(\frac{I}{I_0}\right)^{s_I^{N:C}}. \quad (2)$$

For both ratios, the environmental drivers are concentrations of phosphate ($[PO_4]$) and nitrate ($[NO_3]$), temperature (T), and light (I). The sensitivity factors (s_{driver}^{ratio}, where *ratio* is either P:C or N:C, and *driver* is one of the four environmental drivers) are the exponents that indicate the strength and sign of the drivers. The reference values for the environmental drivers are indicated with subscript 0 in Equations 1 and 2. Also, $[P:C]_0$ and $[N:C]_0$ are the reference stoichiometric values. In our original description of the power law model (Tanioka & Matsumoto, 2017), we described P:C as a function of $[PO_4]$ only, so Equations 1 and 2 represent substantially expanded versions that encompass N as well. Dividing N:C by P:C yields N:P, so the entire C:N:P can now be determined as a function of the four environmental drivers.

Table 1
Sensitivity Factors of the C:N:P Power Law Model

		Eukaryotes		Cyanobacteria		Diazotrophs	
		$[P:C]_0$	$[N:C]_0$	$[P:C]_0$	$[N:C]_0$	$[P:C]_0$	$[N:C]_0$
Reference ratio (‰)		11.6	151.0	6.3	151.0	6.3	151.0
		Eukaryotes		Cyanobacteria		Diazotrophs	
Environmental driver	Reference value	$S^{P:C}_{driver}$	$S^{N:C}_{driver}$	$S^{P:C}_{driver}$	$S^{N:C}_{driver}$	$S^{P:C}_{driver}$	$S^{N:C}_{driver}$
$[PO_4]$	0.57 μmol kg^{-1}	0.58		0.28		0.28	
$[NO_3]$	5.7 μmol kg^{-1}		0.22		0.22		
Temperature	291°K (18 °C)			−8.0		−8.0	
Light	70 W m^{-2}		−0.05		−0.05		−0.05

Note. The sensitivity factors express the dependence of P:C and N:C on environmental drivers according to Equations (1) and (2) in the main text. They were determined by a recent meta-analysis (Tanioka & Matsumoto, 2020a). The reference values for drivers $[PO_4]$, $[NO_3]$, and temperature are global annual mean from the top 100 m in the World Ocean Atlas (H. E. Garcia et al., 2014; Locarnini et al., 2013). The reference light value of 70 W m^{-2} is the global annual mean photosynthetically active radiation in MESMO. Reference ratios $[P:C]_0 = 11.6‰$ (i.e., C:P = 86.2) for eukaryotes and $[P:C]_0 = 6.3‰$ (i.e., C:P = 158.7) for cyanobacteria and diazotrophs are recast from Tanioka and Matsumoto (2017) at reference $[PO4]_0 = 0.57$ μmol kg^{-1}. Reference $[N:C]_0 = 151.0‰$ for all phytoplankton types is the Redfield ratio (i.e., C:N = 106:16).

Compared to the linear model of P:C (Galbraith & Martiny, 2015), the power law model predicts a strong frugality behavior in P utilization under oligotrophic conditions and saturation under eutrophic conditions (Tanioka & Matsumoto, 2017). For example, at the Bermuda Atlantic Time-series Study (BATS) station in the oligotrophic North Atlantic subtropical gyre (Martiny et al., 2013), measurements show a $[PO_4]$ ~0.1–0.01 μmol kg^{-1} and P:C ~4‰ (or C:P ~229:1). Whereas the linear model would substantially underestimate C:P (149–165) for $[PO_4]$ ~0.1–0.01 μmol kg^{-1}, the frugality behavior of the power law model at such low $[PO_4]$ predicts much higher C:P (149–303), more consistent with observations. The power law model likewise performs better when compared to the Hawaii Ocean Time Series (HOTS) station data. At the high end of $[PO_4]$, the power law model would eventually predict stabilization of P:C, as one might expect in cells with finite storage capacity. In contrast, the linear model will predict ever increasing P:C without bound. Numerically, the power law formulation can easily represent fixed stoichiometries such as the Redfield ratio by equating s^{ratio}_{driver} to zero and $[P:C]_0$ and $[N:C]_0$ to the Redfield values.

The challenge in expanding the original power law model of P:C to the model of P:N:C as a function of four environmental drivers is that the sensitivity factors in Equations 1 and 2 were not well constrained or understood. The existing literature included numerous studies of how phytoplankton stoichiometry depends on different drivers, sometimes with a conflicting sense of change. They also studied different strains of algae often under dissimilar conditions. In order to overcome this challenge and in a separate study, we conducted an exhaustive meta-analysis of laboratory studies of marine phytoplankton stoichiometry in order to quantify the sensitivity factors (Tanioka & Matsumoto, 2020a). Meta-analysis is a powerful statistical framework for synthesizing multiple, independent studies and uncovering trends, and it follows rigorous formal protocols to ensure reproducibility and reduce bias (Gurevitch et al., 2018).

Our meta-analysis analyzed 241 experimental units of P:C and 366 experimental units of N:C encompassing seven taxonomic phyla (Tanioka & Matsumoto, 2020a), which we translated to the three PFTs represented in our biogeochemistry model for this study (Table 1). In our meta-analysis, we also examined Fe as a possible driver, but there was an insufficient number of experimental units to determine the sensitivity factor for Fe. Note in Table 1 that s^{ratio}_{driver} does not exist for all combinations of ratios and drivers, as some drivers were not significant. According to the power law definition, s^{ratio}_{driver} indicates the fractional change in the ratio for a fractional change in the driver. For example, $s^{P:C}_{[PO_4]} = 0.58$ for eukaryotes means that a 1% increase in $[PO_4]$ leads to a 0.58% increase in P:C. Our meta-analysis indicates that $s^{P:C}_{[PO_4]}$ for eukaryotes is larger than for cyanobacteria or diazotrophs. One of the ways by which this difference can be understood is in terms of the larger size and storage capacity of eukaryotes that allow luxury storage of P. Where s^{ratio}_{driver} is negative, the sense of change

Table 2
Experiments With Glacial Boundary Conditions

						MOC		MLD					
			Air T	pCO_2	Sea ice	Atl	SO	N. Atl	SO	POC	Deep O_2	Nfix	Den
Experiments	Description	ID	°C	μatm	%	Sv	Sv	m	m	PgC	μmol kg^{-1}	TgN $year^{-1}$	TgN $year^{-1}$
Control	Modern	190917a	13.6	279	10.5	12.0	41.7	176	426	9.4	157	109	109
LGM	Full glacial	190917g	8.3	225	17.2	14.8	20.5	304	322	8.9	131	202	206
BC_Ice	Glacial land ice	190917h	11.2	264	13.3	13.5	42.1	233	429	8.9	169	100	99
BC_Rad	GHG = −2.6 W m^{-2}	190917i	10.9	259	13.8	11.5	42.3	199	440	8.6	174	81	77
BC_Dust	Glacial dust	190917k	13.2	257	11.1	12.1	41.8	173	439	10.9	134	172	174
BC_Orbital	Glacial orbital	190917x	13.8	283	10.5	11.8	41.6	174	430	9.4	158	109	109
BC_Winds	−50% SH westerlies	190917j	13.2	269	11.1	12.7	20.3	174	296	8.4	136	145	147

Note. All results represent the end state after 5,000 years of model integration. Air T = global annual mean surface air temperature. Sea ice indicates the global annual mean sea ice coverage. MOC = meridional overturning circulation, separated into the Atlantic (Atl) and the Southern Ocean (SO). Sv = 10^6 m s^{-3}. MLD = mixed layer depth. POC = global POC export across 100 m water depth. PgC = 10^{15} grams C. Deep O_2 = global mean dissolved O_2 in the interior ocean. Nfix = global N_2 fixation rate. Den = global water column denitrification rate. TgN = 10^{12} grams N. pCO_2 feedback on climate is "off" where BC_Rad (GHG = greenhouse gas forcing) is applied.

in the ratio is opposite. For example, $s_T^{P:C} = -8.0$ for cyanobacteria and diazotrophs indicates that a 1% increase in temperature (in terms of °K) leads to an 8% drop in P:C. While this may appear to be a very large sensitivity, a 1% change in °K is actually large in °C (i.e., ~3°C) and thus represents a very large forcing not easily realized in the real ocean. There are a number of reasons why phytoplankton become more C rich under warmer conditions, including increased metabolic stimulation of C fixation. The interested reader is referred to the meta-analysis (Tanioka & Matsumoto, 2020a) for a discussion of the underlying biochemical reasons for the sense and magnitude of s_{driver}^{ratio}.

We also carried out experiments with two other formulations of C:N:P for comparison. The first is the fixed, default ratio of C:N:P = 117:16:1 that is applied to all three PFTs in the experiment Redfield. The second experiment GM is based on the model of Galbraith and Martiny (2015), where P:C is a linear function of $[PO_4]$ and N:C is a Holland type 2 functional form with a frugality behavior only at very low $[NO_3]$. The same P:C and N:C formulations were applied to all three PFTs. Note that our GM experiments are not the same as those of Ödalen et al. (2020), who did not include the N:C flexibility of Galbraith and Martiny (2015).

Finally, we clarify that the C:N:P ratio calculated for each PFT by Equations 1 and 2 is the ratio during uptake (i.e., organic matter production). We thus consider this to be the physiological control on flexible stoichiometry to be distinguished from the taxonomic control defined below. Since there is no preferential remineralization of nutrients in the model, the calculated uptake ratio could be considered the ratio of biomass. However, as noted above, PFTs in this model technically have no biomass. Also, if there were only a single vertical level in the production layer, the uptake C:N:P ratio would be identical to the export C:N:P ratio. In this model, however, there are two levels within the production layer, and this causes the uptake ratio to become decoupled from the export ratio. The combination of the differences in nutrient concentrations, temperature, and light availability in the vertical levels leads to a higher uptake C:N:P ratio in the top level compared to the second level everywhere. The export ratio is the average of the uptake ratios from both levels, weighted by their contributions to the total POC export. When the uptake stoichiometry is fixed (e.g., Redfield ratio), it is identical to the export ratio, so the decoupling of the two ratios is a notable feature of employing a flexible C:N:P stoichiometry in this study.

2.3. Glacial Boundary Conditions

In this study, we applied five different LGM boundary conditions (BCs, Table 2): (1) larger land ice albedo; (2) reduced radiative forcing from greenhouse gases; (3) insolation changes due to Earth's orbital parameters; (4) increased Fe from dust deposition; and (5) weaker southern hemisphere westerly winds. During LGM, Laurentide and Fenno-Scandinavian Ice Sheets covered large parts of North America and Eurasia that are ice-free today. In experiment BC_Ice, a uniform land ice albedo is thus assigned to grid points according to glacial ice sheet reconstructions (Peltier, 1994). In experiment BC_Rad, we adjusted the radiative forcing in the equilibrium run by −2.6 W m^{-2}, which represents the difference in forcing from three greenhouse gas concentrations (CO_2, CH_4, and N_2O) between LGM and the late Holocene (Fortunat Joos &

Table 3
LGM Sensitivity Experiments

(a)

			POC Export									
				Eukary	Cyano	Diaz		Opal	$CaCO_3$	Deep O_2	Nfix	Den
Experiments	Description	ID	PgC	PgC (%)	PgC (%)	PgC (%)	C:N:P	Tmol Si	PgC	μmol kg^{-1}	TgN $year^{-1}$	TgN $year^{-1}$
Control	Modern	190917a	9.4	3.6 (39)	4.9 (52)	0.8 (9)	113:16:1	128	0.6	157	109	109
LGM	Full glacial	190917g	8.9	6.3 (70)	1.9 (21)	0.7 (8)	140:16:1	89	0.9	131	202	206
LGM_CNP	LGM C:N:P mask	190917q	8.1	5.9 (72)	1.7 (21)	0.6 (7)	126:17:1	86	0.8	142	153	154
LGM_COM	LGM COM mask	190917r	9.4	3.1 (33)	5.3 (57)	0.9 (10)	147:17:1	62	0.6	122	243	245
C_Redfield	Redfield control	190917e	9.0	4.8 (53)	3.6 (40)	0.6 (7)	117:16:1	124	0.6	164	78	78
LGM_Redfield	C:N:P = 117:16:1	190917o	7.4	5.5 (74)	1.4 (19)	0.5 (7)	117:16:1	77	0.6	156	105	106
C_GM	GM control	190917f	8.9	4.1 (47)	4.0 (45)	0.8 (8)	107:16:1	126	0.6	163	91	91
LGM_GM	Linear C:P	190917p	7.8	5.7 (73)	1.5 (19)	0.6 (8)	120:18:1	91	0.7	146	140	141

(b)

		PFT C:N:P							Surface nutrients			
	pCO_2					fPOP	fPOP	BE	PO_4	NO_3	Si	FeT
Experiments	μatm	COM	Eukary	Cyano	Diaz			%	μmol kg^{-1}	μmol kg^{-1}	μmol kg^{-1}	μmol kg^{-1}
Control	279	146:19:1	102:14:1	198:23:1	213:32:1	1.00	1.00	0	0.31	2.7	2.2	0.16
LGM	225	166:18:1	152:16:1	211:21:1	210:32:1	0.77	0.95	79	0.26	2.1	20.5	0.49
LGM_CNP	240	139:17:1	124:15:1	203:23:1	202:31:1	0.77	0.87	41	0.25	2.2	26.3	0.56
LGM_COM	195	180:20:1	132:15:1	219:22:1	239:36:1	0.76	0.99	98	0.26	2.3	43.2	0.37
C_Redfield	279	117:16:1	117:16:1	117:16:1	117:16:1	1.00	1.00	0	0.31	2.6	2.5	0.23
LGM_Redfield	245	117:16:1	117:16:1	117:16:1	117:16:1	0.83	0.83	0	0.27	2.1	32.4	0.67
C_GM	279	119:18:1	109:17:1	130:19:1	131:19:1	1.00	1.00	0	0.28	2.9	2.1	0.22
LGM_GM	234	128:19:1	126:19:1	135:20:1	133:19:1	0.78	0.88	45	0.26	2.5	21.9	0.62

Note. All results represent the end state after 5,000 years of model integration. Global annual mean. Eukary = eukaryotes; cyano = cyanobacteria; diaz = diazotrophs. POC Export % in parentheses indicates the fractional contribution of each PFT to the total community export in terms of NPP carbon. BC_Rad is applied to all glacial experiments, and thus pCO2 feedback is "off." COM = phytoplankton community. The COM stoichiometry is calculated over the production layer (<100 m) and weighted by NPP measured in terms of P instead of C of PFTs. fPOP = particulate organic phosphorus export normalized to control run; likewise for fPOC. BE = Buffer effect according to Equation 4 in the main text.

Spahni, 2008). In experiment BC_Orbit, insolation received by Earth was adjusted according to the glacial orbital parameters (Berger, 1978). An important BC for biology is the increase in aeolian flux of Fe as a result of a dustier glacial atmosphere. In experiment BC_Dust, we applied a reconstruction of glacial dust flux (Mahowald et al., 2006) assuming the same iron content and solubility. Finally, in experiment BC_Winds, we reduced southern westerly wind stress poleward of 44°S by 50%. This follows the idea that the Southern Ocean ventilation is key to modulating atmospheric pCO_2 on glacial cycles, and it is the reduction in ventilation that contributes substantially to lowering pCO_2 during peak glacial times (e.g., Anderson et al., 2009; Sigman et al., 2010; Skinner et al., 2010; Toggweiler et al., 2006). A reduction in southern westerlies as a means to achieve the desired change in Southern Ocean ventilation is an accepted model practice (e.g., Jeltsch-Thömmes et al., 2019; Tschumi et al., 2008). Here we adopt the same practice but do not necessarily believe that a 50% reduction in southern westerly wind stress actually occurred. We note that coupled model results are mixed on how the southern westerlies changed during the last glacial period: strengthening and poleward displacement (Wyrwoll et al., 2000), weakening and equatorward shift (Kim et al., 2003), and insubstantial shift in position with modest weakening (Rojas et al., 2009) or slight strengthening (Otto-Bliesner et al., 2006). In experiment LGM, all five glacial BCs were applied simultaneously to the global model.

3. Results

Three equilibrium model states were obtained for the three formulations of C:N:P (power law, Redfield, and GM) so as to remove model drift in subsequent experiments. From each equilibrium run, we carried out 5,000 years of Control and LGM runs. For the power law formulation, additional 5,000-year sensitivity

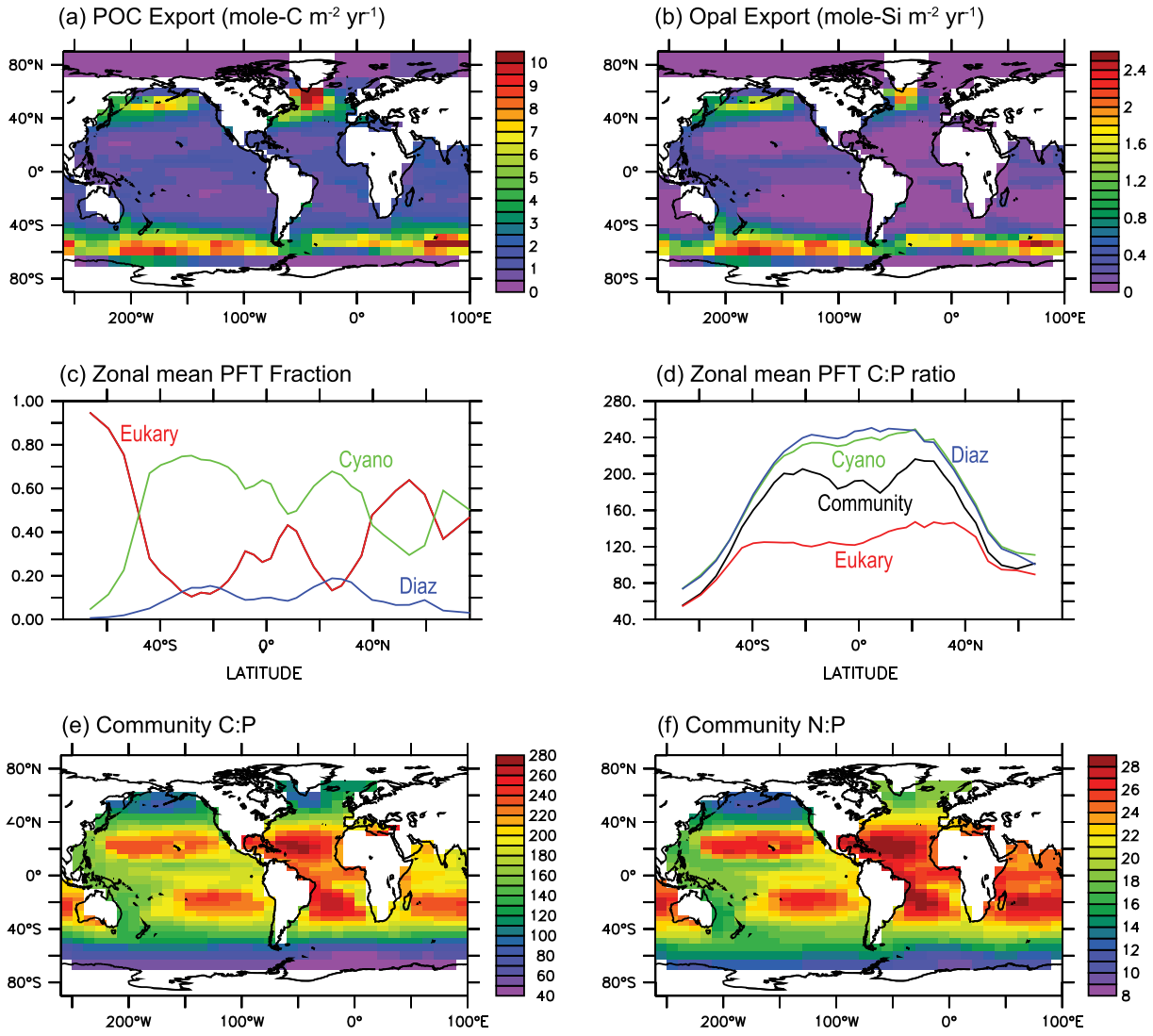

Figure 1. Annual mean properties in the Control experiment: (a) POC export (mole-C m^{-2} $year^{-1}$), (b) opal export (mole-Si m^{-2} $year^{-1}$), (c) zonal mean PFT community composition (fraction), (d) zonal mean PFT C:P, (e) community C:P, and (f) community N:P. The zonal means (c, d) and the vertically averaged community C:P and N:P ratios (e, f) are weighted by NPP of PFTs over the production layer. In (c) and (d), red = eukaryotes, green = cyanobacteria, blue = diazotrophs, and black = community.

experiments were carried out. They include experiments where glacial BCs are applied one at a time (Table 2) as well as experiments where two production masks have been applied to the LGM run (Table 3).

3.1. Control Run With the Power Law Model of C:N:P

The Control run for MESMO2 with the power law model of C:N:P (Figure 1, Tables 2 and 3) is reasonable globally when compared to the original MESMO2 (Matsumoto et al., 2013) and available observations. For example, the model simulates global export production of 9.4 Pg-C $year^{-1}$ of POC, 128 Tmol-Si $year^{-1}$ of opal, and 0.6 Pg-C $year^{-1}$ of $CaCO_3$, compared respectively to data-based estimates of 9.6 ± 3.6 Pg-C $year^{-1}$, 101 ± 35 Tmol-Si $year^{-1}$, and 0.52 ± 0.15 Pg-C $year^{-1}$ (Dunne et al., 2007). Spatially, carbon and opal export productions are large in eutrophic subpolar waters and elevated in the equatorial upwelling regions (Figures 1a and 1b). In those waters, the fast-growing eukaryote PFT typically makes the largest contribution to the community NPP as expected (red line, Figure 1c). In contrast, eukaryotes are the least dominant PFT in the subtropical gyres, whose low nutrient concentrations favor cyanobacteria (green line). Diazotrophs are the least important (blue line).

The power law model predicts higher C:N:P for all PFTs with decreasing latitudes (Figure 1d), as temperature increases, and nutrients become generally depleted. The eukaryotes have the lowest C:N:P, while the other two PFTs representing smaller cells have much higher C:N:P. The stoichiometry of the phytoplankton community at each ocean grid location is calculated as the PFT- and NPP-weighted average over the production layer:

$$C{:}N{:}P_{community} = \frac{\sum_{i,k} C{:}N{:}P(i,\,k) \cdot NPP(i,\,k)}{\sum_{i,k} NPP(i,\,k)}, \tag{3}$$

where i is the PFT index and k is the depth index in the production layer. In Equation 3, NPP is based on P, which is the model currency of nutrient uptake. Thus, the most dominant PFT will exert the greatest control over the local community stoichiometry (black line, Figure 1d). This is the taxonomic or community composition control on stoichiometry as opposed to the physiological control exemplified in Equations 1 and 2. Thus, in the subtropical gyres, the combination of smaller PFTs' higher C:N:P and their taxonomic dominance results in high community C:N:P (Figures 1e and 1f) as observed (Martiny et al., 2013).

Globally, the power law model predicts the lowest C:N:P for eukaryotes (102:14:1) and much higher ratios (C:N:P = 198–213:23–32:1) for cyanobacteria and diazotrophs (Table 3). The global mean phytoplankton community C:N:P is 146:19:1. In comparison, the global C:N:P of export production is 113:16:1, which is close to the canonical Redfield ratio.

It is important to note for this study that the Control run also preserves some of the realistic representation of the marine silica cycle achieved in MESMO2 (Matsumoto et al., 2013). With the introduction of Fe-dependent, variable Si:N, MESMO2 was able to trap silicic acid in the Southern Ocean sourced circulation loop and deplete it in the surface waters globally (Sarmiento et al., 2004). As a result, the PFT that represents diatoms is limited by silicic acid for much of the world ocean except in the Southern Ocean where Fe is limiting (Figure 2a). This feature allowed MESMO2 to simulate the silicic acid leakage (Matsumoto et al., 2014), a phenomenon speculated to have occurred during the last glacial period (Brzezinski et al., 2002; Matsumoto et al., 2002). In contrast, cyanobacteria in the Control run are limited by nitrate for much of the world ocean except by Fe in the Southern Ocean (Figure 2c). Diazotrophs are mostly limited by Fe except by phosphate in the Atlantic Ocean (Figure 2e).

Finally, diazotrophs fix N globally at the rate of 109 Tg-N year^{-1} within the model, which is in good agreement with available range of estimates (Landolfi et al., 2018). It is balanced by denitrification in the Control run. The whole ocean ratio between nitrate and phosphate inventories is 15.4 in the model. In comparison, the estimated global water column denitrification rate is 60–150 Tg-N year^{-1} (Bianchi et al., 2018; Codispoti, 2007; Devries et al., 2012) and global ocean N:P ratio is ~15 (Tyrrell, 1999).

3.2. Effects of the Glacial Boundary Conditions

Of the five glacial BCs, changes in radiative forcing owing to much lower greenhouse gas concentrations cause the greatest cooling (Table 2). Global mean surface air temperature decreases by 2.7 °C from 13.6 °C in the Control run to 10.9 °C in BC_Rad. The next coldest climate is predicted by experiment BC_Ice, where air temperature cools by 2.4 °C. Changes in orbital parameters, dust, and winds do not cool the planet substantially. The cooling realized by the glacial land ice albedo and radiative forcing enhances gas solubility, which lowers atmospheric pCO_2 by 15–20 μatm and increases deep ocean [O_2] by 12–17 μmol kg^{-1}. If it were not for the expanded global sea ice coverage, which increases by 27–31%, deep [O_2] would have increased even more. Increased Fe flux in experiment BC_Dust has a substantial biological fertilization effect. The change in global POC export, which is driven mostly by net eukaryotic growth, increases from 9.4 to 10.9 Pg-C year^{-1}. This contrasts with POC export reduction in all other glacial BC experiments. The increased biological pump in BC_Dust leads to atmospheric pCO_2 drawdown by 22 μatm as well as deep [O_2] reduction by 23 μmol kg^{-1}. In experiment BC_Winds, a 50% weakening of the southern westerlies wind stress substantially reduces Southern Ocean ventilation, as the Southern Ocean mixed layer depth (MLD) shoals by 130 m from 426 m and as the southern overturning drops from 41.7 Sv (Sv = 10^6 m^3 s^{-1}) to 20.3 Sv. Reduced ventilation diminishes the supply of dissolved O_2 to the ocean interior, so that deep [O_2]

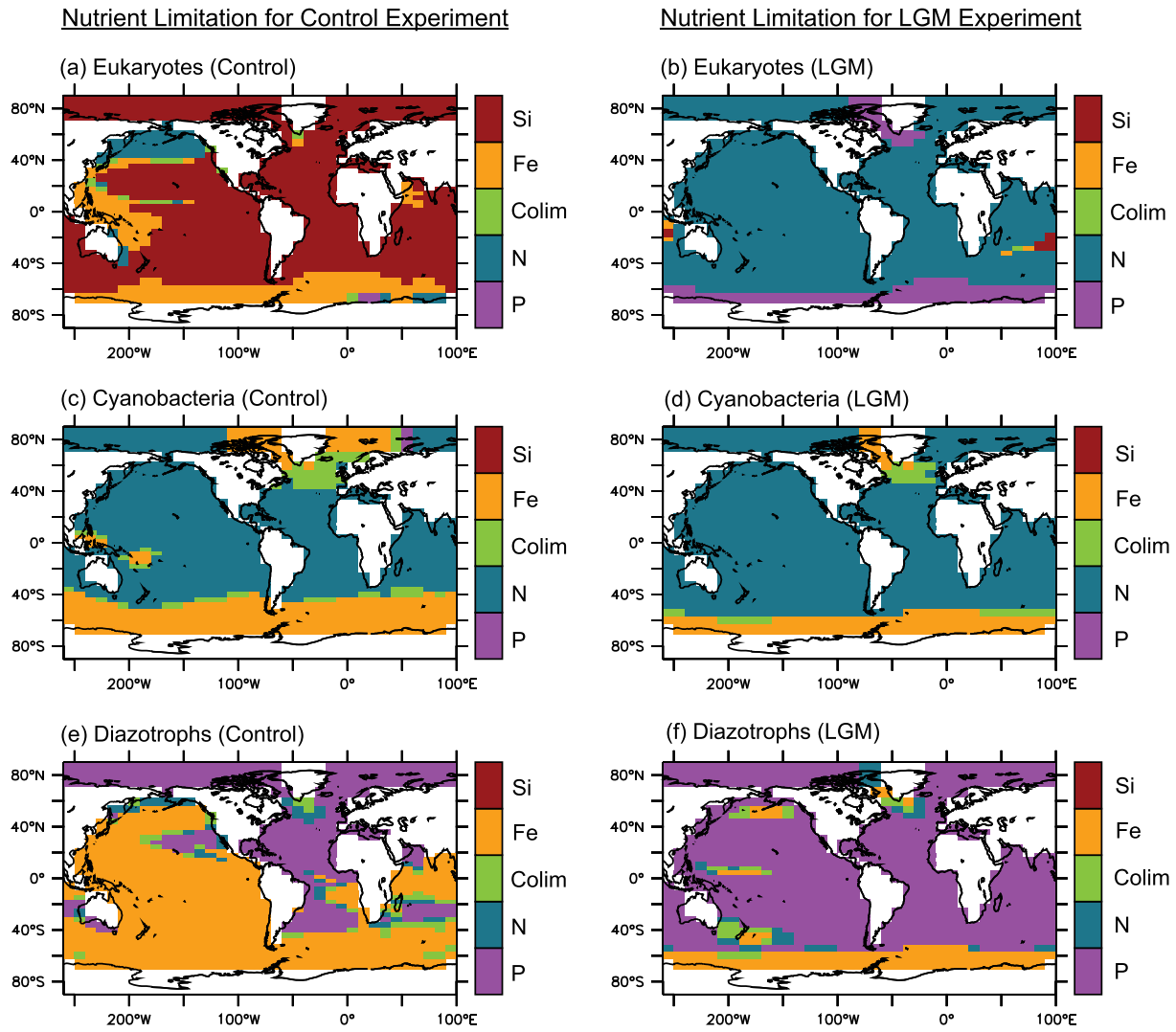

Figure 2. Annual mean nutrient limitation maps for Control run (a) eukaryotes, (c) cyanobacteria, (e) diazotrophs, and LGM run (b) eukaryotes, (d) cyanobacteria, (f) diazotrophs. Limitations: 1 = phosphate, 2 = nitrate, 3 = co-limitation; 4 = iron, and 5 = silicic acid.

is reduced by 21 μmol kg^{-1}. Finally, changes in the orbital parameters in experiment BC_Orbit cause minimal change in insolation with no appreciable impact on model physics and biogeochemistry.

The changes listed in Table 2 have been described for the model with the power law model of flexible C:N:P. When the same BCs are applied to models with the Redfield C:N:P or GM formulation of C:N:P, the physical changes (e.g., cooling ventilation) are quantitatively comparable, and the biogeochemical changes (e.g., POC export, deep O_2) have the sense of change.

3.3. LGM Run

When all glacial BCs are simultaneously applied to the model in the experiment LGM, many of the individual effects described for controlled BC experiments are superimposed to give larger changes (Figure 3, Table 2). As a result, global surface air temperature cools by 5.3°C, atmospheric pCO_2 is reduced by 54 μatm, polar sea ice expands by 64%, global POC export decreases by 0.5 Pg-C $year^{-1}$, and deep ocean [O_2] drops by 26 μmol kg^{-1}. The drop in deep [O_2] occurs despite the greater gas solubility that leads to higher [O_2] in surface waters, where expanded sea ice does not inhibit air-sea gas exchange (Figure 4). Since the global POC export decreases in the experiment LGM, much of the drop in deep ocean [O_2] is largely attributable to reduced southern winds driving weaker ventilation. Nevertheless, there is a dust

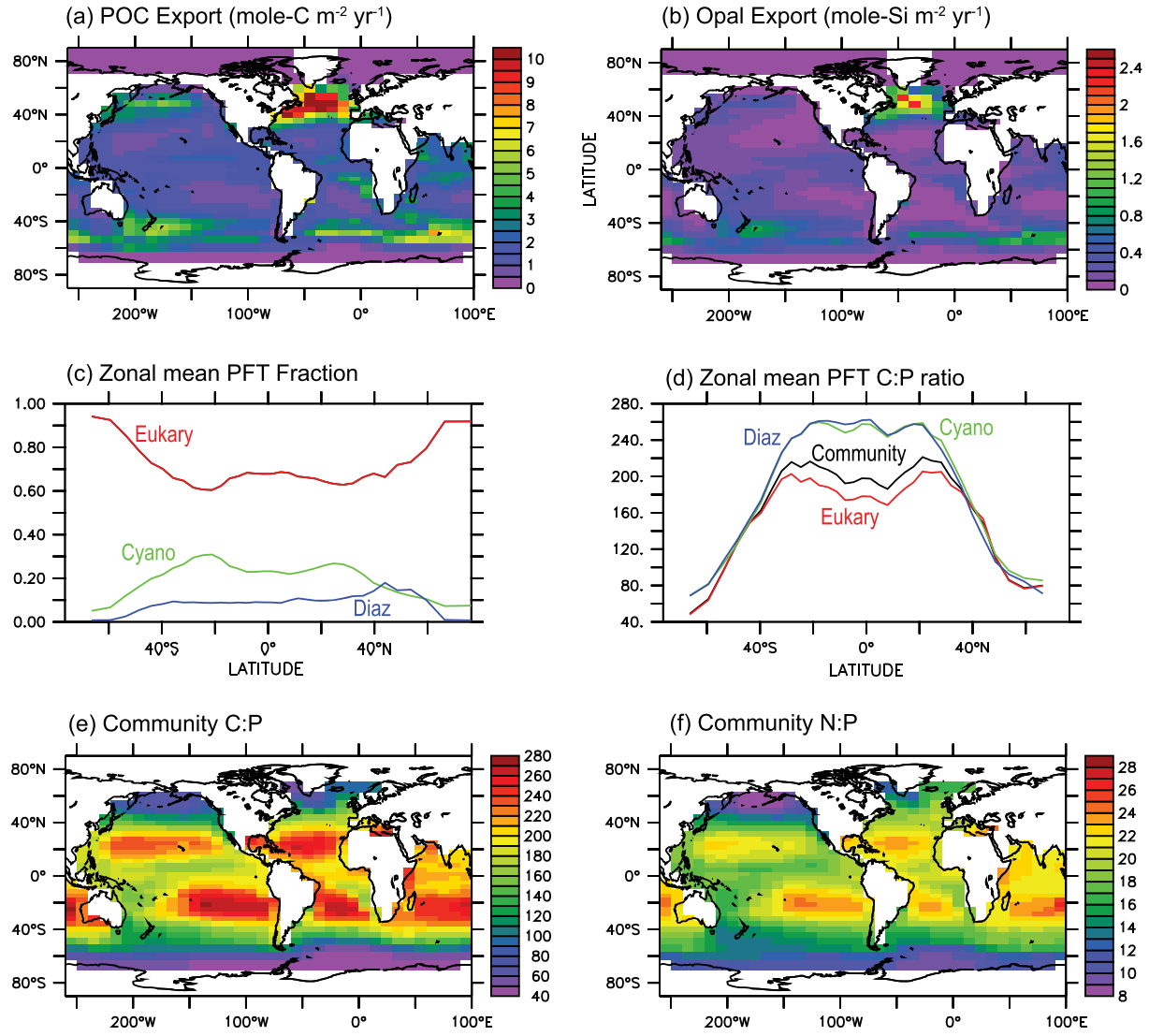

Figure 3. Annual mean properties in the LGM experiment. See Figure 1 caption for details.

component to the deep [O_2] reduction, because the global POC export would have been much lower without the Fe fertilization effect. The two indices of Southern Ocean ventilation point to weakening as the Southern Ocean MLD shoals by 104 m and overturning decreases by 20.2 Sv.

There are two physical changes in the experiment LGM compared to the Control run that have important consequences for phytoplankton stoichiometry (Table 3). The first is the large expansion of sea ice, which notably reduces the Southern Ocean contribution to the global production (Figure 5). In the Control run, diatoms dominate the Southern Ocean, whose POC export accounts for one third of global export production. In comparison, the Southern Ocean contribution is estimated by data analysis and inverse modeling to be 10–30% (Dunne et al., 2007; Schlitzer, 2002). Given their low C:N:P, the Southern Ocean diatoms thus have the effect of lowering global export C:N:P. Therefore, when Southern Ocean sea ice expands and suppresses eukaryote production, the global export C:N:P becomes increasingly decoupled from the low Antarctic diatom C:N:P. The global export C:N:P increases from 113:16:1 in the Control run to 140:16:1 in the LGM run. There is thus a 24% increase in the carbon content in the sinking POM per unit P with important implications for buffering of changes in carbon export.

The second important physical change in the LGM experiment is the increased input of Fe from glacial dust deposition. Fe has a direct fertilization effect that increases production of all PFTs in places where Fe is

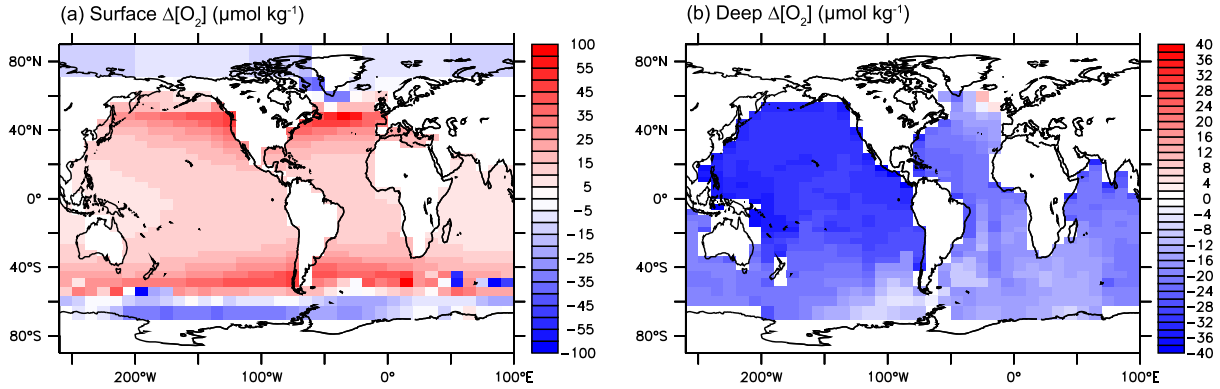

Figure 4. LGM-Control change in dissolved oxygen: (a) surface and (b) 2,000–5,000 m. Unit is μmol kg^{-1}.

limiting. More importantly in this study, the Fe input reduces the Si:N uptake ratio by diatoms, so that silicic acid becomes available in much of the world's surface ocean in a manner previously hypothesized (Brzezinski et al., 2002; Matsumoto et al., 2002) and predicted (Matsumoto et al., 2014). This relieves the severe silicic acid limitations to diatom growth, thus boosting POC production of eukaryotes outside areas of expanded sea ice (Figure 6a). The global eukaryote POC export thus increases by 2.7 Pg-C $year^{-1}$ from 3.6 to 6.3 Pg-C $year^{-1}$ (Tables 2 and 3). Because eukaryotes have high V_{max}, this growth comes at the expense of cyanobacteria growth (Figure 6b) and helps deplete surface nutrients. The global mean surface $[PO_4]$ decreases from 0.31 to 0.26 μmol-P kg^{-1} with a larger change in the Pacific (Figure 6c). Again, this occurs outside the polar waters where phosphate actually increases due to suppression of biological production by sea ice. Surface mean nitrate concentration also decreases globally but even under expanded sea ice (Figure 6d). This reduction in nitrate beyond that in phosphate reflects reduced oceanic N inventory, because the drop in the deep ocean $[O_2]$ enhances denitrification globally. By the end of the 5,000-year run, the deep ocean $[NO_3]$ is down from 33 to 30 μmol-N kg^{-1} and still dropping, because the global N_2 fixation has not caught up to the change in global denitrification. The global ocean inventory ratio of N:P drops from 15.4 in the Control run to 13.9 at the end of the LGM run. As a result, eukaryotes and cyanobacteria both become largely limited by nitrate (Figure 2; see Table 3 for surface nutrient concentrations).

There are two implications for phytoplankton stoichiometry from these changes triggered by increased Fe input (Figure 7). First, the depletion of nutrients has the effect of elevating C:N:P according to the power law model of flexible stoichiometry. This physiological response is strongest in the eukaryote's C:P (Figure 7a), which has the greatest sensitivity to phosphate with $s^{P:C}_{[PO_4]} = 0.58$. As a result, the global mean C:N:P for eukaryotes increases from 102:14:1 to 152:16:1 (Table 3). Cyanobacteria and diazotrophs have the same sense of response but weaker ($s^{P:C}_{[PO_4]} = 0.28$), and their overall C:P is also negatively affected by

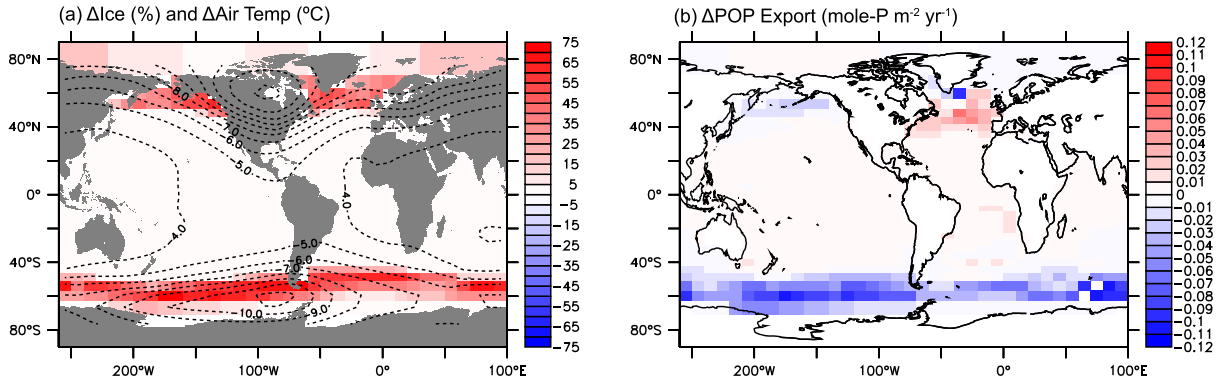

Figure 5. LGM-Control change. (a) Ice fraction (%, color) and surface mean air temperature (°C, contour line). (b) POP export (mole-P m^{-2} $year^{-1}$).

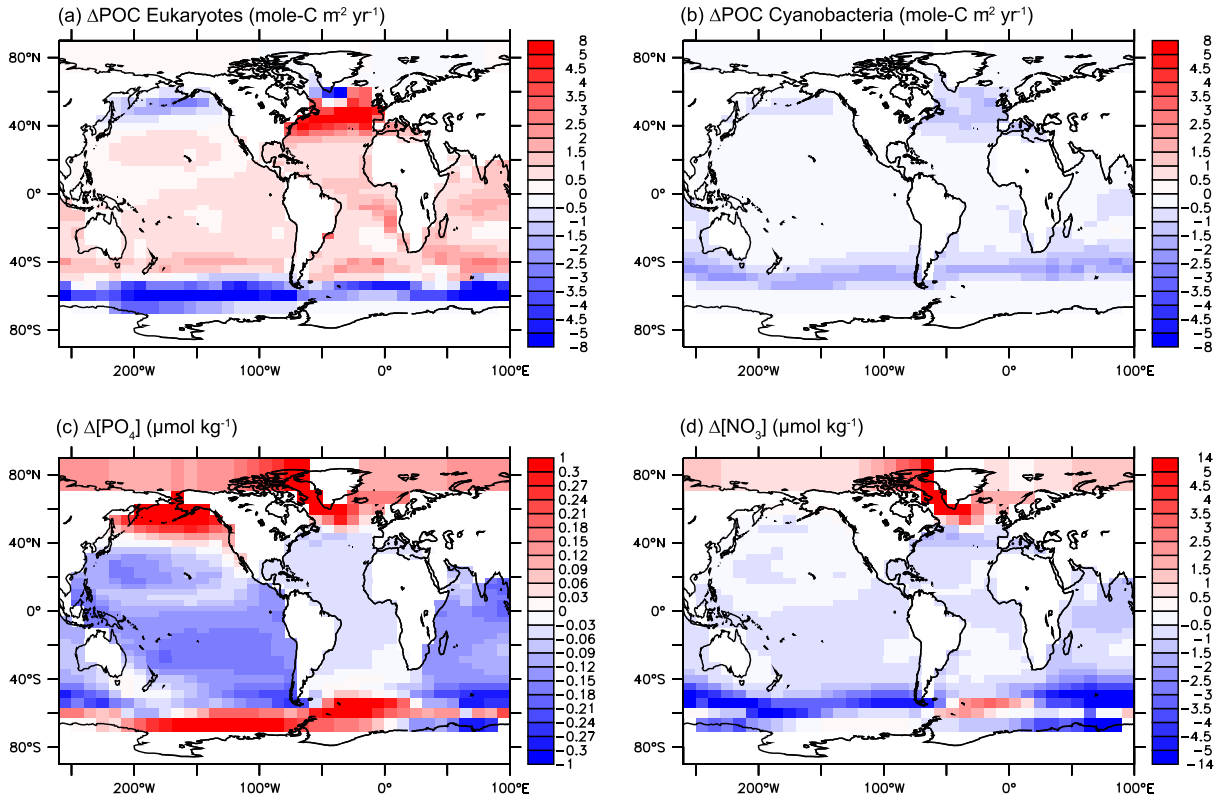

Figure 6. LGM-Control change. POC export (mole-C m^{-2} year^{-1}) by (a) eukaryote PFT and (b) cyanobacteria PFT. Change in nutrient concentrations (μmol kg^{-1}) over the production layer for (c) phosphate and (d) nitrate.

cooling ($s_T^{P:C} = -8.0$). Thus, the change in C:P for cyanobacteria and diazotrophs under glacial conditions is more mixed than for eukaryotes (Figures 7b and 7c). The physiological response in the C:N ratio is very much analogous to C:P in that reduced surface [NO_3] (Figure 6d) causes C:N to rise in both eukaryotes and cyanobacteria, both having $s_{[NO_3]}^{N:C} = 0.22$ (Figure 7d; only eukaryote C:N shown). The second implication is that as eukaryotes become the dominant PFT under glacial BCs, the local community C:N:P decreases and approaches C:N:P of eukaryotes (Table 3). This is clearly seen in the case for C:P under glacial conditions compared to the Control run (i.e., community C:P in black line is much closer to eukaryote C:P in red line in Figure 3d than in Figure 1d).

The globally elevated export production C:N:P in the LGM run indicates that stoichiometric buffering of POC export should occur. This buffering can be quantified by comparing POC that is expected from particulate organic phosphorus (POP) export assuming fixed stoichiometry versus the POC export actually simulated with flexible C:N:P. In the LGM run, global POP export declined by 23% (fPOP = 0.77, Table 3; Figure 5b), but global POC export declines only by 5% (fPOC = 0.95). In comparison, global POP and POC export changes by the same fraction in the experiment LGM_Redfield (i.e., fPOP = fPOC = 0.83, Table 3).

A measure of the buffer effect (BE) can be quantified with the following equation:

$$BE = \left(1 - \frac{1 - fPOC}{1 - fPOP}\right) \cdot 100. \quad (4)$$

For the experiment LGM_Redfield, where fPOP = fPOC, BE = 0%, indicating no buffering. A hypothetical perfect buffering (i.e., BE = 100%) occurs when POC remains unchanged (i.e., fPOC = 1) for any change in POP due to flexible C:N:P. The LGM experiment has an intermediate but strong buffering response, where fPOP = 0.77 and fPOC = 0.95; thus BE is 79% (Table 3). In the experiment LGM_GM, BE is lower at 45%. BE calculated with respect to particulate organic nitrogen (PON) instead of POP is the same or lower: 79% for LGM, 14% for LGM_GM, and of course 0% for LGM_Redfield.

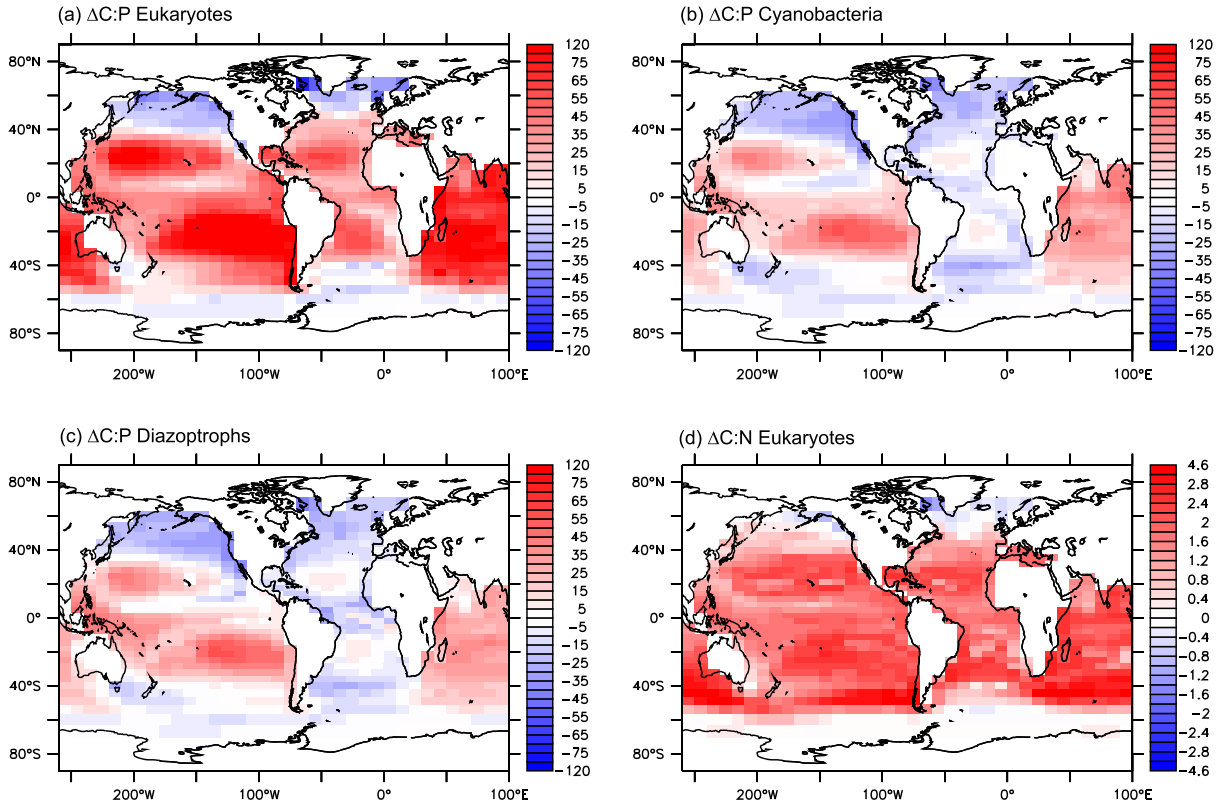

Figure 7. LGM-Control change in phytoplankton PFT stoichiometry over the production layer. (a) Eukaryote C:P, (b) cyanobacteria C:P, (c) diazotroph C:P, and (d) eukaryote C:N.

One would expect that an elevated export C:N:P under glacial conditions would facilitate a greater oceanic uptake of CO_2, thus helping to explain the low glacial atmospheric pCO_2. The change in atmospheric pCO_2 between the Control and LGM runs is 54 μatm. The fraction of 54 μatm that is attributable to flexible stoichiometry is not easily quantified, however, because it is difficult to isolate the different components (e.g., physiology, taxonomy, and regional production) of flexible C:N:P.

The simplest quantification is to compare the 54 μatm reduction to the 34 μatm reduction obtained between the control and glacial runs of the Redfield experiments (Table 3). At face value, the comparison would indicate that having flexible stoichiometry reduces pCO_2 by an additional 20 μatm. However, this 20 μatm also reflects to some degree the fact that the Control runs with fixed C:N:P and flexible C:N:P are not identical (Table 3). For example, the global POC export is 9.0 Pg-C $year^{-1}$ with fixed C:N:P but 9.4 Pg-C $year^{-1}$ with flexible C:N:P.

3.4. LGM Masked Productions Runs

In an effort to more precisely quantify the CO_2 effect of flexible stoichiometry under glacial BCs, we devised two additional sensitivity experiments. In experiment LGM_CNP, we repeated the LGM run, except we applied seasonal masks of C:N:P created from the Control run, so that the seasonal C:N:P cycle for each PFT is repeated everywhere. Likewise, in experiment LGM_COM, seasonal masks of community composition created from the Control run were applied at every grid point. These two new runs are thus intended to be controlled experiments of the LGM run, where LGM_CNP is different from the LGM in only the physiological control on C:N:P, and where LGM_COM is different from LGM in only the taxonomic control on C:N:P.

LGM_CNP successfully works as designed in that the C:N:P of PFT is pegged to the Control run (Figure S2a), while other aspects of the model remain similar to the LGM run, including the community composition (Figure S2b) and surface nutrients (Table 3). Atmospheric pCO_2 in LGM_CNP is 240 μatm, which is 15

μatm higher than in the LGM experiment. We may thus conclude that allowing the physiological C:N:P response to glacial conditions lowers atmospheric pCO_2 by 15 μatm.

In contrast, LGM_COM does not work as well as a control experiment of the LGM run. The problem is that the environmental conditions (e.g., nutrients and light) in the model under glacial conditions are not able to support the exact phytoplankton community composition demanded by the masks. For example, there may not be enough silicic acid to support a large fraction of eukaryotes that the masks may demand. In such a case, the model can only simulate as large a fraction of eukaryotes as possible. As a result, the eukaryote fraction in LGM_COM mostly follows that of the Control run but not perfectly (Figure S2b). At the same time, C:N:P of PFTs in LGM_COM may be quite different from LGM (Figure S2a). LGM_COM is thus somewhat different from LGM in both physiology and taxonomy, not just in taxonomy as designed. Atmospheric pCO_2 in LGM_COM is 195 μatm, which is 30 μatm lower than in the LGM experiment. At face value, we would conclude that the taxonomic response to glacial conditions increases atmospheric pCO_2 by 30 μatm. Although this number is uncertain, the sense of change in pCO_2 is correct in that the general shift in community composition from cyanobacteria to eukaryotes lowers C:N:P ratio. All else being the same, this taxonomic effect would reduce oceanic uptake of CO_2, leading to higher atmospheric pCO_2. The experiments LGM_CNP and LGM_COM thus indicate that the effects of physiology and community composition work in opposite directions under glacial conditions.

4. Discussion

4.1. Controls on Local and Global C:N:P

Our results demonstrate that broadly there are three controls on phytoplankton stoichiometry: physiology, taxonomy, and regional production. First, there is the physiological control on C:N:P for each type of PFT. The sensitivity of the physiological control is different for different PFTs (Table 1). Of the five glacial BCs, increased dust deposition has a notably strong impact on this physiological control through a sequence of events. Starting with increased dust deposition, increased Fe availability ultimately substantially boosts POC production of eukaryote PFT. The fast-growing eukaryotes deplete surface PO_4 and NO_3 to a greater extent in the LGM run than in the Control run (Figures 6c and 6d). The depletion leads to a strong increase in C:P and C:N in eukaryotes (Figures 7a and 7d). Averaged over the production layer globally, eukaryotic C:P is 152:1 in the LGM run compared to 102:1 in the Control (Table 3). In comparison, the increase in C:P in cyanobacteria and diazotrophs by PO_4 depletion is tempered by the cooling effect on C:P.

The second control on phytoplankton C:N:P is taxonomy (Figure 1d), which under glacial BCs becomes increasingly dominated by eukaryotes (Figure 6a). Because eukaryotes have the lowest C:N:P among the three PFTs, the community C:N:P (i.e., average C:N:P weighted by the NPP) declines and approaches C:N:P of eukaryotes in many parts of the world ocean (compare Figures 1d and 7). The physiological and taxonomic controls thus interact locally to determine the community C:N:P at each grid point.

The third control, regional production, acts globally on the phytoplankton stoichiometry. Subtropical gyres have high community C:N:P because cyanobacteria are taxonomically dominant and all PFTs have relatively elevated C:N:P due to low nutrient availability. In contrast, polar regions have lower community C:N:P because eukaryotes are dominant and all PFTs have lower C:N:P due to high nutrient availability. The global export C:N:P is determined by the relative balance of export contributions from subtropical gyres, polar waters, and other regions of the world ocean. Under glacial BCs, the expansion of sea ice diminishes substantially the Southern Ocean contribution to the global export production (Figure 5b), thereby raising the global export stoichiometry.

The importance of the regional production can also be illustrated by comparing global mean phytoplankton C:N:P calculated with and without weighting by NPP. The global mean phytoplankton C:P in the Control run is 146:1 with NPPP weighting and 173:1 without. The difference is directly attributable to eukaryotes in the polar waters making a large contribution to the global NPPP. Also, in the LGM run, C:P is 166:1 with NPPP weighting and 176:1 without. The change in NPPP-weighted C:P between the Control and LGM runs (166–146 = 20) is much larger than the change in the unweighted C:P by (176–173 = 3). This difference indicates that it is the diminished Southern Ocean production in the LGM experiment that accounts for much of the increase in global export C:P from 113:1 to 140:1.

The literature generally supports the notions of sea ice expansion and diminished Antarctic productivity during the last glacial period. For example, diatom-based reconstruction of sea ice indicates that the maximum limit of Antarctic winter sea ice extended northward by 5°–10° latitude in all sectors of the Southern Ocean (Crosta et al., 1998). A reduced biological production is expected to underutilize surface nutrients and lead to increases in their concentrations. This increase is indicated by different nutrient proxies in glacial Antarctic waters: foraminiferal Cd/Ca for [PO_4] (Elderfield & Rickaby, 2000), diatom δ^{30}Si for silica acid (De La Rocha et al., 1998), and δ^{13}C of organic matter bound to diatoms (Rosenthal et al., 2000; Shemesh et al., 1993). For years, these three indices have been considered to be at odds with sedimentary and diatom bound δ^{15}N, which indicate greater NO_3 consumption (Franois et al., 1997; Robinson & Sigman, 2008; Wang et al., 2017). Our modeling results suggest a possible reconciliation of these apparently contradictory results regarding glacial Southern Ocean nutrient utilization. We posit that nitrate becomes decoupled from the other nutrients in the Southern Ocean. That is, despite lowered productivity associated with sea ice expansion leading to increased surface water PO_4, silicic acid, and lighter δ^{13}C, surface [NO_3] decreases in the model (Figure 6). This is a result of the drop in deep ocean [O_2] enhancing denitrification and the low NO_3 signal propagating even into surface waters that are largely under expanded sea ice.

4.2. Carbon Implications of Flexible C:N:P

In this study, the global mean export C:N:P increased from 113:16:1 in the Control run to 140:16:1 in the LGM run. When broken down into C:P and C:N, the Control run has C:P = 113:1 and C:N = 6.9, and the LGM run has C:P = 140:1 and C:N = 8.5. There are a number of implications for the global increase in both C:P and C:N, but in particular there are two for carbon. First, the increase in C:N:P facilitates stoichiometric buffering of POC export. In the LGM run, in which the power law model of flexible stoichiometry was employed, POP export dropped by 23%, and POC export dropped by just 5% (Table 3). According to Equation 4, the magnitude of buffering or BE is 79%. With a fixed, Redfield stoichiometry, BE is 0%; with the GM formulation of stoichiometry, BE is 45%. The power law model, which has a larger dynamic range of C:N:P and better matches the BATS and HOTS data than the other two formulations, indicates that stochiometric buffering of POC export is substantially larger.

Second, some of the reduction in atmospheric pCO_2 under glacial conditions is due to flexible C:N:P. A simple comparison of the LGM runs with the power law model and Redfield ratio indicates that flexible stoichiometry is responsible for ~20 μatm reduction overall. The sensitivity experiment LGM_CNP, which controls for the physiological aspect of C:N:P variability, indicates that ~15 μatm reduction can be accounted for by physiology. Most of the physiological effect is from C:P increasing with decreasing [PO_4]. The experiment LGM_COM suggests that the taxonomic effect (i.e., a shift away from cyanobacteria in favor of eukaryotes, thus lowering C:N:P) would increase pCO_2 by ~30 μatm. We are not able to quantify the effect of regional production changes on atmospheric pCO_2, but it is likely large given that NPPP-weighting of global C:P averaging increases C:P substantially. The overall reduction in pCO_2, which may be ~20 μatm, would be some combination of pCO_2 reductions from physiology and regional production and an pCO_2 increase from taxonomy.

Ödalen et al. (2020), who employed a linear C:P formulation and a single PFT, also report a reduction in atmospheric pCO_2 attributable to flexible stoichiometry under glacial conditions. Their reduction is smaller, 8-16 μatm, which may be a result of a number of differences between the two studies. One difference is that the maximum achievable C:P in their study is 167, which is too low compared to observations, so their physiological effect (i.e., pCO_2 reduction) is likely underestimated. Also, since the taxonomic control is likely to increase pCO_2, missing it entirely with a single PFT has the effect of reducing pCO_2. Another important difference is that in our model, the glacial Fe input triggers the silicic acid leakage, which cannot be simulated without the marine silica cycle.

Since this study is focused on the effect of flexible stoichiometry on the ocean carbon cycle, a comprehensive discussion of the full glacial-interglacial pCO_2 amplitude of 80–100 μatm is beyond the scope of this study. Furthermore, we did not consider carbonate compensation, a major mechanism of pCO_2 change (Broecker & Peng, 1987). We note though that 20 μatm is comparable to other major mechanisms such as solubility (Sigman & Boyle, 2000) and therefore suggest that flexible phytoplankton stoichiometry could be one, currently overlooked, component of the mix of mechanisms to explain the full amplitude.

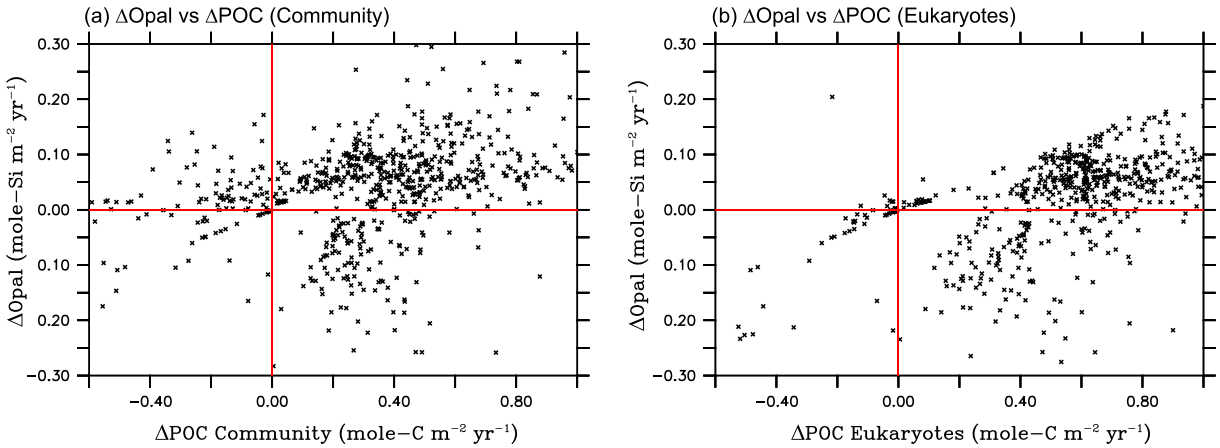

Figure 8. LGM-Control change in opal export versus POC export at ocean grid points. (a) ΔOpal vs ΔPOC of community. (b) ΔOpal vs ΔPOC of eukaryotes. Unit: opal export = mole-Si m^{-2} $year^{-1}$, POC export = mole-C m^{-2} $year^{-1}$.

4.3. Implications for Oxygen, Opal, and Nitrogen

The increase in phytoplankton C:P and C:N ratios under glacial BCs have implications and lessons beyond just carbon. One of them is for oxygen, more specifically the export O_2:C ratio, which links changes in interior ocean [O_2] to the amount of respired carbon sequestered. This ratio is tied to C:N such that an increase in C:N leads to a decrease in O_2:C (Peng & Broecker, 1987; Tanioka & Matsumoto, 2020b):

$$O_2{:}C = 1.11 + 2/C{:}N. \tag{5}$$

In the model, the global C:N export ratio increases from approximately 6.9 to 8.5. According to Equation 5, O_2:C is expected to decrease from the modern value of 1.40 to 1.35, a drop by ~4%, which is indeed simulated by the model. This drop reflects the fact that organic matter produced under glacial conditions is predicted to be more carbon rich (i.e., rich in carbohydrates and poorer in proteins) than today, and carbohydrates require less oxygen for complete respiration (O_2:C~1.0) than proteins (O_2:C > 1.0) (Anderson, 1995). The change in the respiration ratio has important implications for the derivation of the amount of carbon sequestered in the glacial ocean.

Recent paleo-proxy studies have determined that many parts of the glacial ocean including the deep Atlantic and equatorial Pacific Ocean during the last glacial period had substantially lower [O_2] than today (Anderson et al., 2019; Hoogakker et al., 2015; Lu et al., 2016). Our model too predicts deoxygenation in the ocean interior (Figure 4b). In the Pacific, apparent oxygen utilization was 153 μmol-O_2 kg^{-1} greater during the glacial period (Anderson et al., 2019). Assuming that O_2:C remained unchanged and using O_2:C = 1.414, the study estimated that respiratory carbon was greater during the glacial period by 108 μmol-C kg^{-1} in concentration and by 850 Pg-C in ocean inventory. Our results would suggest that the respiration ratio used for this estimate should be 4% lower. This would increase the estimated respiratory carbon inventory by ~34 Pg-C, which translates to approximately 17 μatm in atmospheric pCO_2.

The silicic acid implication of this study is that the reduction in Si:N uptake ratio by diatoms can decouple opal production from POC production under glacial BCs. As noted, the sequence of events starting from increased Fe input boosts global eukaryote POC export by 2.7 Pg-C $year^{-1}$, a 75% increase. In contrast, total POC export by all PFTs combined decreases by 0.5 Pg-C $year^{-1}$, a modest 5% drop, while global opal export declines sharply by 39 Tmol-Si $year^{-1}$, a 30% change. There is thus a substantial decoupling at the global level between opal and POC export fluxes. Locally, the relationships between those fluxes can be even more variable (Figure 8). The traditional expectation is that the change in POC and opal fluxes are positively related (quadrants 1 and 3, Figures 8a and 8b). However, there are locations (e.g., North Pacific) where the total POC export and eukaryote POC export increases but opal export decreases (quadrant 4, Figures 8a and 8b). In some locations (e.g., South Indian), the total POC export can decrease but opal export can increase (quadrant 2, Figure 8a). The local decoupling supports the argument that

increased opal flux would not necessarily be a consequence of the silicic acid leakage (Matsumoto & Sarmiento, 2008). Figure 8 indicates that taxonomy also has a role in decoupling total POC export from opal export.

Finally, there are some implications for the N cycle. As the glacial deep ocean becomes substantially deoxygenated (Robert F. Anderson et al., 2019; Hoogakker et al., 2015; Lu et al., 2016), a strong enhancement of denitrification is expected. Our model indeed predicts deoxygenation (Figure 4b) and denitrification, which nearly doubles to 206 Tg-N $year^{-1}$ by the end of the 5,000 years of the LGM experiment (Table 3). The reduction in both oceanic N inventory and thus N:P ratio in seawater gives competitive advantage to diazotrophs and enhances their efficiency of N_2 fixation. This helps diazotrophs maintain their production unlike cyanobacteria and increase N_2 fixation (Table 3). By the end of the run, global N_2 fixation is 202 Tg-N $year^{-1}$, not quite on a par with denitrification. In the surface ocean, $[NO_3]$ declines by 0.6 μmol-N kg^{-1} in the LGM run compared to the Control run. When the dynamic N cycle is turned off in the model, surface $[NO_3]$ is reduced by 0.4 μmol-N kg^{-1}, which is due to enhanced eukaryote growth under glacial conditions. Thus, approximately one third of the 0.6 μmol-N kg^{-1} decline can be attributed to the transient change in the global ocean N inventory. This change accounts for a minor fraction of the C:N increase seen in eukaryote and cyanobacteria PFTs.

Our prediction of enhanced global water column denitrification under glacial conditions appears to be at odds with the isotopically light $\delta^{15}N$ data from major sites of water column denitrification today (Altabet et al., 1995; Ganeshram et al., 1995). Those data have traditionally been interpreted to indicate reduced water column denitrification but are not necessarily indicative of globally reduced denitrification, since there could be significant denitrification in other glacial low O_2 zones of the ocean. Similarly, a recent modeling study suggests that sedimentary denitrification combined with N_2 fixation could explain those lighter $\delta^{15}N$ data (Buchanan et al., 2019). Our model does not include N isotopes, but our results would not be inconsistent with this suggestion. Interestingly, the modeling work of Buchanan et al. (2019) and this work are similar in that enhanced Fe input is prescribed as a glacial BC, yet the response of the nitrogen cycle is somewhat dissimilar. In their work, global N_2 fixation is also stimulated by denitrification and low N:P ratio, and this extra source of nitrate in the eastern equatorial Pacific leads to a more complete consumption of surface phosphate, higher C:P in non-diazotrophs, and a net drawdown of atmospheric pCO_2. Whereas their global N_2 fixation rate increases by 26 Tg-N $year^{-1}$, it increases by nearly 90 Tg-N $year^{-1}$ in this study. Yet this does not increase the oceanic N inventory in our LGM run, because the global denitrification rate is always greater than the global N_2 fixation rate. In our model, the enhanced growth of eukaryotes is stimulated by the relief of silicic acid limitation. Probably one of the important technical differences between their work and ours is that we have two PFTs that separately represent eukaryotes and cyanobacteria with different nutrient limitations, whereas they have one "general" PFT that represents both groups of phytoplankton with very different physiological attributes.

5. Conclusions

Modern observations clearly point to variations in phytoplankton stoichiometry on ocean basin scale. The power law model offers an effective way by which C:N:P flexibility can be incorporated into a global ocean model. Our results indicate that under glacial conditions, an increase in global C:N:P strongly buffers POC export from change and contributes to approximately 20 μatm of atmospheric CO_2 drawdown. These findings suggest that flexible stoichiometry is an important driver of ocean carbon cycle on glacial-interglacial timescale.

We have identified three key controls on what determines export C:N:P ratio. At the local level, phytoplankton physiology and community structure are important. At the global level, the balance in regional production becomes critical. Sea ice expansion and Fe input are important in modifying these controls under glacial conditions.

We did not explicitly model how phytoplankton C:N:P is modified by preferential remineralization of N and P by heterotrophy. This was the mechanism that prompted Weyl to suggest to Broecker that a rise in export C:P could help explain low glacial atmospheric pCO_2. It is not clear how specifically glacial conditions could have altered heterotrophy to bring about the needed rise in export C:P, but a preferential release of nutrients

over carbon from sinking organic matter in the modern ocean is well recognized (e.g., Shaffer, 1996). In our model food web interactions including heterotrophy could be yet another control on export C:N:P and the biological pump.

A number of our model results agree with available paleo records, for example, of expanded sea ice, reduced phosphate, and silicic acid utilization in Antarctic waters, but increased apparent nitrate utilization associated with the decreased nitrogen inventory, and increased production elsewhere. Our results showed that opal flux and POC flux can be decoupled locally, and this points to the difficulty in characterizing production by paleo proxies. There is as yet no verified paleo proxy of phytoplankton C:N:P. If such a proxy were developed, a whole new subfield of paleo research may open up.

Data Availability Statement

Model results have been archived with the Biological & Chemical Oceanography Data Management Office (BCO-DMO) and available freely (https://www.bco-dmo.org/dataset/784634).

Acknowledgments
This work is dedicated to Wally Broecker who passed away in February 2019. His first papers on the biological pump revolutionized paleo and chemical oceanography and spawned many investigations including this work. This work was supported by the U.S. National Science Foundation (OCE-1827948). K.M. was supported by the Leverhulme Trust Visiting Professorship while on sabbatical at the University of Oxford. R. R. acknowledges support from ERC Consolidator Grant APPELS (ERC-2015-COG-681746) and a Wolfson Research Merit Award. Numerical modeling and analysis were carried out using resources at the University of Minnesota Supercomputing Institute.

References

Altabet, M. A., Francois, R., Murray, D. W., & Prell, W. L. (2020). Climate-related variations in denitrification in the Arabian Sea from sediment15N/14N ratios. *Nature*, *373*(6514), 506–509. https://doi.org/10.1038/373506a0

Anderson, L. A. (1995). On the hydrogen and oxygen content of marine phytoplankton. *Deep Sea Research Part I: Oceanographic Research Papers*, *42*(9), 1675–1680. https://doi.org/10.1016/0967-0637(95)00072-E

Anderson, L. A., & Sarmiento, J. L. (1994). Redfield ratios of remineralization determined by nutrient data analysis. *Global Biogeochemical Cycles*, *8*(1), 65–80. https://doi.org/10.1029/93GB03318

Anderson, R. F., Ali, S., Bradtmiller, L. I., Nielsen, S. H. H., Fleisher, M. Q., Anderson, B. E., & Burckle, L. H. (2009). Wind-driven upwelling in the Southern Ocean and the deglacial rise in atmospheric CO_2. *Science*, *323*(5920), 1443–1448. https://doi.org/10.1126/science.1167441

Anderson, R. F., Sachs, J. P., Fleisher, M. Q., Allen, K. A., Yu, J., Koutavas, A., & Jaccard, S. L. (2019). Deep-sea oxygen depletion and ocean carbon sequestration during the last ice age. *Global Biogeochemical Cycles*, *33*, 301–317. https://doi.org/10.1029/2018GB006049

Archer, D., Eby, M., Brovkin, V., Ridgwell, A., Cao, L., Mikolajewicz, U., et al. (2009). Atmospheric lifetime of fossil fuel carbon dioxide. *Annual Review of Earth and Planetary Sciences*, *37*(1), 117–134. https://doi.org/10.1146/annurev.earth.031208.100206

Archer, D., Winguth, A., Lea, D., & Mahowald, N. (2000). What caused the glacial/interglacial atmospheric pCO_2 cycles? *Reviews of Geophysics*, *38*(1999), 159–189. https://doi.org/10.1029/1999RG000066

Arora, V., Katavouta, A., Williams, R., Jones, C., Brovkin, V., Friedlingstein, P., et al. (2019). Carbon-concentration and carbon-climate feedbacks in CMIP6 models, and their comparison to CMIP5 models. *Biogeosciences Discussions*, (December), 1–124. https://doi.org/10.5194/bg-2019-473

Balch, W. M., Bates, N. R., Lam, P. J., Twining, B. S., Rosengard, S. Z., Bowler, B. C., et al. (2016). Factors regulating the Great Calcite Belt in the Southern Ocean and its biogeochemical significance. *Global Biogeochemical Cycles*, *30*, 1124–1144. https://doi.org/10.1002/2016GB005414

Barnola, J. M., Raynaud, D., Korotkevich, Y. S., & Lorius, C. (1987). Vostok ice core provides 160,000-year record of atmospheric CO_2. *Nature*, *329*(6138), 408–414. https://doi.org/10.1038/329408a0

Berger, A. L. (1978). Long-term variations of daily insolation and quaternary climatic changes. *Journal of Atmospheric Science*, *35*(12), 2362–2367. https://doi.org/10.1175/1520-0469(1978)035<2362:ltvodi>2.0.co;2

Bianchi, D., Weber, T. S., Kiko, R., & Deutsch, C. (2018). Global niche of marine anaerobic metabolisms expanded by particle microenvironments. *Nature Geoscience*, *11*(4), 263–268. https://doi.org/10.1038/s41561-018-0081-0

Bopp, L., Resplandy, L., Orr, J. C., Doney, S. C., Dunne, J. P., Gehlen, M., et al. (2013). Multiple stressors of ocean ecosystems in the 21st century: Projections with CMIP5 models. *Biogeosciences*, *10*(10), 6225–6245. https://doi.org/10.5194/bg-10-6225-2013

Broecker, W. S. (1982a). Glacial to interglacial changes in ocean chemistry. *Progress in Oceanography*, *11*(2), 151–197. https://doi.org/10.1016/0079-6611(82)90007-6

Broecker, W. S. (1982b). Ocean chemistry during glacial time. *Geochimica et Cosmochimica Acta*, *46*(10), 1689–1705. https://doi.org/10.1016/0016-7037(82)90110-7

Broecker, W. S., & Henderson, G. M. (1998). The sequence of events surrounding termination II and their implications for the cause of glacial-interglacial CO_2 changes. *Paleoceanography*, *13*(4), 352–364. https://doi.org/10.1029/98PA00920

Broecker, W. S., & Peng, T. H. (1982). *Tracers in the sea*. Palisades: Eldigio Press. https://doi.org/10.1016/0016-7037(83)90075-3

Broecker, W. S., & Peng, T.-H. (1987). The role of $CaCO_3$ compensation in the glacial to interglacial atmospheric CO_2 change. *Global Biogeochemical Cycles*, *1*(1), 15–29. https://doi.org/10.1029/GB001i001p00015

Brzezinski, M. A., Pride, C. J., Franck, V. M., Sigman, D. M., Gruber, N., Rau, G. H., & Coale, K. H. (2002). A switch from $Si(OH)_4$ to NO_3^- depletion in the glacial Southern Ocean. *Geophysical Research Letters*, *29*(12), https://doi.org/10.1029/2001GL014349

Buchanan, P. J., Chase, Z., Matear, R. J., Phipps, S. J., & Bindoff, N. L. (2019). Marine nitrogen fixers mediate a low latitude pathway for atmospheric CO_2 drawdown. *Nature Communications*, *10*(1), 4611. https://doi.org/10.1038/s41467-019-12549-z

Cao, L., Eby, M., Ridgwell, A., Caldeira, K., Archer, D., Ishida, A., et al. (2009). The role of ocean transport in the uptake of anthropogenic CO_2. *Biogeosciences*, *6*(3), 375–390. https://doi.org/10.5194/bg-6-375-2009

Codispoti, L. A. (2007). An oceanic fixed nitrogen sink exceeding 400 Tg N a-1 vs the concept of homeostasis in the fixed-nitrogen inventory. *Biogeosciences*, *4*(2), 233–253. https://doi.org/10.5194/bg-4-233-2007

Crosta, X., Pichon, J. J., & Burckle, L. H. (1998). Reappraisal of Antarctic seasonal sea-ice at the Last Glacial Maximum. *Geophysical Research Letters*, *25*(14), 2703–2706. https://doi.org/10.1029/98GL02012

Daines, S. J., Clark, J. R., & Lenton, T. M. (2014). Multiple environmental controls on phytoplankton growth strategies determine adaptive responses of the N:P ratio. *Ecology Letters*, *17*(4), 414–425. https://doi.org/10.1111/ele.12239

De La Rocha, C. L., Brzezinski, M. A., DeNiro, M. J., & Shemesh, A. (1998). Silicon-isotope composition of diatoms as an indicator of past oceanic change. *Nature*, *395*(6703), 680–683. https://doi.org/10.1038/27174

Devries, T., Deutsch, C., Primeau, F., Chang, B., & Devol, A. (2012). Global rates of water-column denitrification derived from nitrogen gas measurements. *Nature Geoscience*, *5*(8), 547–550. https://doi.org/10.1038/ngeo1515

Droop, M. R. (1974). The nutrient status of algal cells in continuous culture. *Journal of the Marine Biological Association of the United Kingdom*, *54*(4), 825–855. https://doi.org/10.1017/S002531540005760X

Dunne, J. P., Sarmiento, J. L., & Gnanadesikan, A. (2007). A synthesis of global particle export from the surface ocean and cycling through the ocean interior and on the seafloor. *Global Biogeochemical Cycles*, *21*, GB4006. https://doi.org/10.1029/2006GB002907

Eby, M., Weaver, A. J., Alexander, K., Zickfeld, K., Abe-Ouchi, A., Cimatoribus, A. A., et al. (2013). Historical and idealized climate model experiments: An intercomparison of Earth system models of intermediate complexity. *Climate of the Past*, *9*(3), 1111–1140. https://doi.org/10.5194/cp-9-1111-2013

Elderfield, H., & Rickaby, R. E. M. (2000). Oceanic Cd/P ratio and nutrient utilization in the glacial Southern Ocean. *Nature*, *405*(6784), 305–310. https://doi.org/10.1038/35012507

Falkowski, P. G. (1997). Evolution of the nitrogen cycle and its influence on the biological sequestration of CO_2 in the ocean. *Nature*, *387*(6630), 272–275. https://doi.org/10.1038/387272a0

Franck, V. M., Brzezinski, M. A., Coale, K. H., & Nelson, D. M. (2000). Iron and silicic acid concentrations regulate Si uptake north and south of the Polar Frontal Zone in the Pacific Sector of the Southern Ocean. *Deep-Sea Research Part II: Topical Studies in Oceanography*, *47*(15–16), 3315–3338. https://doi.org/10.1016/S0967-0645(00)00070-9

Franois, R., Altabet, M. A., Yu, E.-F. F., Sigman, D. M., Bacon, M. P., Frank, M., et al. (1997). Contribution of Southern Ocean surface-water stratification to low atmospheric CO_2 concentrations during the last glacial period. *Nature*, *389*(6654), 929–935. https://doi.org/10.1038/40073

Galbraith, E. D., & Martiny, A. C. (2015). A simple nutrient-dependence mechanism for predicting the stoichiometry of marine ecosystems. *Proceedings of the National Academy of Sciences*, *112*(27), 8199–8204. https://doi.org/10.1073/pnas.1423917112

Ganeshram, R. S., Pedersen, T. F., Calvert, S. E., & Murray, J. W. (1995). Large changes in oceanic nutrient inventories from glacial to interglacial periods. *Nature*. https://doi.org/10.1038/376755a0

Garcia, C. A., Baer, S. E., Garcia, N. S., Rauschenberg, S., Twining, B. S., Lomas, M. W., & Martiny, A. C. (2018). Nutrient supply controls particulate elemental concentrations and ratios in the low latitude eastern Indian Ocean. *Nature Communications*, *9*(1), 4868. https://doi.org/10.1038/s41467-018-06892-w

Garcia, H. E., Locarnini, R. A., Boyer, T. P., Antonov, J. I., Baranova, O. K., Zweng, M. M., et al. (2014). World Ocean Atlas 2013, Volume 4: Dissolved inorganic nutrients (phosphate, nitrate, silicate). In S. Levitus & A. Mishonov (Eds.), *NOAA Atlas NESDIS 76* (Vol. *4*, pp. 25). NOAA.

Geider, R. J., & La Roche, J. (2002). Redfield revisited: Variability of C:N:P in marine microalgae and its biochemical basis. *European Journal of Phycology*, *37*(1), 1–17. https://doi.org/10.1017/S0967026201003456

Griffies, S. M. (1998). The Gent-McWilliams skew flux. *Journal of Physical Oceanography*, *28*(5), 831–841. https://doi.org/10.1175/1520-0485(1998)028<0831:TGMSF>2.0.CO;2

Gurevitch, J., Koricheva, J., Nakagawa, S., & Stewart, G. (2018). Meta-analysis and the science of research synthesis. *Nature*, *555*(7695), 175–182. https://doi.org/10.1038/nature25753

Heinze, C., Maier-Reimer, E., & Winn, K. (1991). Glacial pCO_2 reduction by the World Ocean: Experiments with the Hamburg carbon cycle model. *Paleoceanography*, *6*(4), 395–430. https://doi.org/10.1029/91PA00489

Hoogakker, B. A. A., Elderfield, H., Schmiedl, G., McCave, I. N., & Rickaby, R. E. M. (2015). Glacial–interglacial changes in bottom-water oxygen content on the Portuguese margin. *Nature Geoscience*, *8*(1), 40–43. https://doi.org/10.1038/ngeo2317

Ilyina, T., Six, K. D., Segschneider, J., Maier-Reimer, E., Li, H., & Núñez-Riboni, I. (2013). Global ocean biogeochemistry model HAMOCC: Model architecture and performance as component of the MPI-Earth system model in different CMIP5 experimental realizations. *Journal of Advances in Modeling Earth Systems*, *5*, 287–315. https://doi.org/10.1029/2012MS000178

Jeltsch-Thömmes, A., Battaglia, G., Cartapanis, O., Jaccard, S. L., & Joos, F. (2019). Low terrestrial carbon storage at the Last Glacial Maximum: Constraints from multi-proxy data. *Climate of the Past*, *15*(2), 849–879. https://doi.org/10.5194/cp-15-849-2019

Joos, F., Roth, R., Fuglestvedt, J. S., Peters, G. P., Enting, I. G., Von Bloh, W., et al. (2013). Carbon dioxide and climate impulse response functions for the computation of greenhouse gas metrics: A multi-model analysis. *Atmospheric Chemistry and Physics*, *13*(5), 2793–2825. https://doi.org/10.5194/acp-13-2793-2013

Joos, F., & Spahni, R. (2008). Rates of change in natural and anthropogenic radiative forcing over the past 20,000 years. *Proceedings of the National Academy of Sciences of the United States of America*, *105*(5), 1425–1430. https://doi.org/10.1073/pnas.0707386105

Kim, S. J., Flato, G. M., & Boer, G. J. (2003). A coupled climate model simulation of the last glacial maximum, Part 2: Approach to equilibrium. *Climate Dynamics*, *20*(6), 635–661. https://doi.org/10.1007/s00382-002-0292-2

Landolfi, A., Kähler, P., Koeve, W., & Oschlies, A. (2018). Global marine N2 fixation estimates: From observations to models. *Frontiers in Microbiology*, *9*(SEP), 1–8. https://doi.org/10.3389/fmicb.2018.02112

Lee, S. Y., Chiang, J. C. H., Matsumoto, K., & Tokos, K. S. (2011). Southern Ocean wind response to North Atlantic cooling and the rise in atmospheric CO_2: Modeling perspective and paleoceanographic implications. *Paleoceanography*, *26*, 1–16. https://doi.org/10.1029/2010PA002004

Locarnini, R. A., Mishonov, A. V., Antonov, J. I., Boyer, T. P., Garcia, H. E., Baranova, O. K., et al. (2013). World Ocean Atlas 2013, Volume 1: Temperature. In S. Levitus & A. Mishonov (Eds.), *NOAA Atlas NESDIS 73* (Vol. *1*, pp. 40).

Lu, Z., Hoogakker, B. A. A., Hillenbrand, C.-D., Zhou, X., Thomas, E., Gutchess, K. M., et al. (2016). Oxygen depletion recorded in upper waters of the glacial Southern Ocean. *Nature Communications*, *7*(7), 11146. https://doi.org/10.1038/ncomms11146

Lüthi, D., Le Floch, M., Bereiter, B., Blunier, T., Barnola, J.-M., Siegenthaler, U., et al. (2008). High-resolution carbon dioxide concentration record 650,000–800,000 years before present. *Nature*, *453*(7193), 379–382. https://doi.org/10.1038/nature06949

Mahowald, N. M., Muhs, D. R., Levis, S., Rasch, P. J., Yoshioka, M., Zender, C. S., & Luo, C. (2006). Change in atmospheric mineral aerosols in response to climate: Last glacial period, preindustrial, modern, and doubled carbon dioxide climates. *Journal of Geophysical Research: Atmospheres*, *111*, D10202. https://doi.org/10.1029/2005JD006653

Martin, J. H. (1990). Iron hypothesis of CO_2 change. *Paleoceanography*, *5*(1), 1–13. https://doi.org/10.1029/PA005i001p00001

Martiny, A. C., Pham, C. T. A., Primeau, F. W., Vrugt, J. A., Moore, J. K., Levin, S. A., & Lomas, M. W. (2013). Strong latitudinal patterns in the elemental ratios of marine plankton and organic matter. *Nature Geoscience*, *6*(4), 279–283. https://doi.org/10.1038/ngeo1757

Matsumoto, K., Chase, Z., & Kohfeld, K. (2014). Different mechanisms of silicic acid leakage and their biogeochemical consequences. *Paleoceanography*, *29*, 1–17. https://doi.org/10.1002/2013PA002588.Received

Matsumoto, K., & Sarmiento, J. L. (2008). A corollary to the silicic acid leakage hypothesis. *Paleoceanography*, *23*. https://doi.org/10.1029/2007PA001515

Matsumoto, K., Sarmiento, J. L., & Brzezinski, M. A. (2002). Silicic acid leakage from the Southern Ocean: A possible explanation for glacial atmospheric $p\,CO_2$. *Global Biogeochemical Cycles*, *16*(3), 5-1–5–23. https://doi.org/10.1029/2001GB001442

Matsumoto, K., Tokos, K., Chikamoto, M., & Ridgwell, A. (2010). Characterizing post-industrial changes in the ocean carbon cycle in an Earth system model. *Tellus Series B: Chemical and Physical Meteorology*, *62*(4), 296–313. https://doi.org/10.1111/j.1600-0889.2010.00461.x

Matsumoto, K., Tokos, K., Huston, A., & Joy-Warren, H. (2013). MESMO 2: A mechanistic marine silica cycle and coupling to a simple terrestrial scheme. *Geoscientific Model Development*, *6*(2), 477–494. https://doi.org/10.5194/gmd-6-477-2013

Matsumoto, K., Tokos, K. S., Price, A. R., & Cox, S. J. (2008). First description of the Minnesota Earth System Model for Ocean biogeochemistry (MESMO 1.0). *Geoscientific Model Development*, *1*(1), 1–15. https://doi.org/10.5194/gmd-1-1-2008

Matsumoto, K., & Yokoyama, Y. (2013). Atmospheric Δ 14 C reduction in simulations of Atlantic overturning circulation shutdown. *Global Biogeochemical Cycles*, *27*, 296–304. https://doi.org/10.1002/gbc.20035

Moreno, A. R., Hagstrom, G. I., Primeau, F. W., Levin, S. A., & Martiny, A. C. (2018). Marine phytoplankton stoichiometry mediates nonlinear interactions between nutrient supply, temperature, and atmospheric CO_2. *Biogeosciences*, *15*(9), 2761–2779. https://doi.org/10.5194/bg-15-2761-2018

Najjar, R. G., Jin, X., Louanchi, F., Aumont, O., Caldeira, K., Doney, S. C., et al. (2007). Impact of circulation on export production, dissolved organic matter, and dissolved oxygen in the ocean: Results from Phase II of the Ocean Carbon-cycle Model Intercomparison Project (OCMIP-2). *Global Biogeochemical Cycles*, *21*, GB3007. https://doi.org/10.1029/2006GB002857

Ödalen, M., Nycander, J., Ridgwell, A., Oliver, K. I., Peterson, C. D., & Nilsson, J. (2020). Variable C/P composition of organic production and its effect on ocean carbon storage in glacial-like model simulations. *Biogeosciences*, *17*(8), 2219–2244. https://doi.org/10.5194/bg-17-2219-2020

Otto-Bliesner, B. L., Brady, E. C., Clauzet, G., Tomas, R., Levis, S., & Kothavala, Z. (2006). Last glacial maximum and Holocene climate in CCSM3. *Journal of Climate*, *19*(11), 2526–2544. https://doi.org/10.1175/JCLI3748.1

Paulsen, H., Ilyina, T., Six, K. D., & Stemmler, I. (2017). Incorporating a prognostic representation of marine nitrogen fixers into the global ocean biogeochemical model HAMOCC. *Journal of Advances in Modeling Earth Systems*, *9*, 438–464. https://doi.org/10.1002/2016MS000737

Peltier, W. R. (1994). Ice age paleotopography. *Science*, *265*(5169), 195–201. https://doi.org/10.1126/science.265.5169.195

Peng, T.-H., & Broecker, W. S. (1987). C/P ratios in marine detritus. *Global Biogeochemical Cycles*, *1*(2), 155–161. https://doi.org/10.1029/GB001i002p00155

Petit, R. J., Raynaud, D., Basile, I., Chappellaz, J., Ritz, C., Delmotte, M., et al. (1999). Climate and atmospheric history of the past 420,000 years from the Vostok ice core, Antarctica. *Nature*, *399*, 429–413. https://doi.org/10.1038/20859

Redfield, A. C. (1934). *On the proportions of organic derivatives in sea water and their relation to the composition of plankton*. Liverpool: University Press of Liverpool, James Johnstone Memorial Volume. https://doi.org/citeulike-article-id:11236440

Redfield, A. C., Ketchum, B. H., & Richards, F. A. (1963). The influence of organisms on the composition of sea-water. In M. N. Hill (Ed.), *The composition of seawater: Comparative and descriptive oceanography. The sea: ideas and observations on progress in the study of the seas*, (pp. 26–77). New York: Interscience Publishers.

Ridgwell, A., Hargreaves, J. C., Edwards, N. R., Annan, J. D., Lenton, T. M., & Marsh, R. (2007). Marine geochemical data assimilation in an efficient Earth System Model of global biogeochemical cycling. *Biogeosciences*, *4*(4), 87–104. https://doi.org/10.5194/bg-4-87-2007

Robinson, R. S., & Sigman, D. M. (2008). Nitrogen isotopic evidence for a poleward decrease in surface nitrate within the ice age Antarctic. *Quaternary Science Reviews*, *27*(9–10), 1076–1090. https://doi.org/10.1016/j.quascirev.2008.02.005

Rojas, M., Moreno, P., Kageyama, M., Crucifix, M., Hewitt, C., Abe-Ouchi, A., et al. (2009). The Southern Westerlies during the last glacial maximum in PMIP2 simulations. *Climate Dynamics*, *32*(4), 525–548. https://doi.org/10.1007/s00382-008-0421-7

Rosenthal, Y., Dahan, M., & Shemesh, A. (2000). Southern ocean contributions to glacial-interglacial changes of atmospheric pCO_2: An assessment of carbon isotope records in diatoms. *Paleoceanography*, *15*(1), 65–75. https://doi.org/10.1029/1999PA000369

Sarmiento, J. L., Gruber, N., Brzezinski, M. A., & Dunne, J. P. (2004). High-latitude controls of thermocline nutrients and low latitude biological productivity. *Nature*, *427*(6969), 56–60. https://doi.org/10.1038/nature02127

Schlitzer, R. (2002). Carbon export fluxes in the Southern Ocean: Results from inverse modeling and comparison with satellite-based estimates. *Deep-Sea Research Part II: Topical Studies in Oceanography*, *49*(9–10), 1623–1644. https://doi.org/10.1016/S0967-0645(02)00004-8

Shaffer, G. (1996). Biogeochemical cycling in the global ocean: 2. New production, Redfield ratios, and remineralization in the organic pump. *Journal of Geophysical Research, Oceans*, *101*(C2), 3723–3745. https://doi.org/10.1029/95JC03373

Shemesh, A., Macko, S. A., Charles, C. D., & Rau, G. H. (1993). Isotopic evidence for reduced productivity in the Glacial Southern Ocean. *Science*, *262*(5132), 407–410. https://doi.org/10.1126/science.262.5132.407

Shuter, B. (1979). A model of physiological adaptation in unicellular algae. *Journal of Theoretical Biology*, *78*(4), 519–552. https://doi.org/10.1016/0022-5193(79)90189-9

Sigman, D. M., & Boyle, E. A. (2000). Glacial/interglacial variations in atmospheric carbon dioxide. *Nature*, *407*(6806), 859–869. https://doi.org/10.1038/35038000

Sigman, D. M., Hain, M. P., & Haug, G. H. (2010). The polar ocean and glacial cycles in atmospheric CO_2 concentration. *Nature*, *466*(7302), 47–55. https://doi.org/10.1038/nature09149

Skinner, L. C., Fallon, S., Waelbroeck, C., Michel, E., & Barker, S. (2010). Ventilation of the deep southern ocean and deglacial CO_2 rise. *Science*, *328*(5982), 1147–1151. https://doi.org/10.1126/science.1183627

Sun, X., & Matsumoto, K. (2010). Effects of sea ice on atmospheric p CO_2: A revised view and implications for glacial and future climates. *Journal of Geophysical Research*, *115*, G02015. https://doi.org/10.1029/2009JG001023

Sunda, W. G., & Huntsman, S. A. (1995). Iron uptake and growth limitation in oceanic and coastal phytoplankton. *Marine Chemistry*, *50*(1–4), 189–206. https://doi.org/10.1016/0304-4203(95)00035-P

Tanioka, T., & Matsumoto, K. (2017). Buffering of ocean export production by flexible elemental stoichiometry of particulate organic matter. *Global Biogeochemical Cycles*, *31*, 1528–1542. https://doi.org/10.1002/2017GB005670

Tanioka, T., & Matsumoto, K. (2020a). A meta-analysis on environmental drivers of marine phytoplankton C: N: P. *Biogeosciences*, *17*(11), 2939–2954. https://doi.org/10.5194/bg-17-2939-2020

Tanioka, T., & Matsumoto, K. (2020b). Stability of marine organic matter respiration stoichiometry. *Geophysical Research Letters*, *47*, 1–10. https://doi.org/10.1029/2019GL085564

Toggweiler, J. R., Russell, J. L., & Carson, S. R. (2006). Midlatitude westerlies, atmospheric CO_2, and climate change during the ice ages. *Paleoceanography*, *21*, PA2005. https://doi.org/10.1029/2005PA001154

Tschumi, T., Joos, F., & Parekh, P. (2008). How important are Southern Hemisphere wind changes for low glacial carbon dioxide? A model study. *Paleoceanography*, *23*, 1–20. https://doi.org/10.1029/2008PA001592

Tyrrell, T. (1999). The relative influences of nitrogen and phosphorus on oceanic primary production. *Nature*, *400*(6744), 525–531. https://doi.org/10.1038/22941

Ushie, H., & Matsumoto, K. (2012). The role of shelf nutrients on glacial-interglacial CO_2: A negative feedback. *Global Biogeochemical Cycles*, *26*, GB2039. https://doi.org/10.1029/2011GB004147

Vichi, M., Pinardi, N., & Masina, S. (2007). A generalized model of pelagic biogeochemistry for the global ocean ecosystem. Part I: Theory. *Journal of Marine Systems*, *64*(1–4), 89–109. https://doi.org/10.1016/j.jmarsys.2006.03.006

Volk, T., & Hoffert, M. I. (1985). Ocean carbon pumps: Analysis of relative strengths and efficiencies in ocean-driven atmospheric CO_2 changes. In E. T. Sundquist & W. S. Broecker (Eds.), *The carbon cycle and atmospheric CO_2: Natural variations Archaen to present* (Vol. Geophysica, pp. 99–110). Washington, DC: American Geophysical Union. https://doi.org/10.1029/GM032p0099

Wang, X. T., Sigman, D. M., Prokopenko, M. G., Adkins, J. F., Robinson, L. F., Hines, S. K., et al. (2017). Deep-sea coral evidence for lower Southern Ocean surface nitrate concentrations during the last ice age. *Proceedings of the National Academy of Sciences*, *114*(13), 3352–3357. https://doi.org/10.1073/pnas.1615718114

Ward, B. A., Wilson, J. D., Death, R. M., Monteiro, F. M., Yool, A., & Ridgwell, A. (2018). EcoGEnIE 1.0: Plankton ecology in the cGEnIE Earth system model. *Geoscientific Model Development*, *11*(10), 4241–4267. https://doi.org/10.5194/gmd-11-4241-2018

Weaver, A. J., Sedlá, J., Eby, M., Alexander, K., Crespin, E., Fichefet, T., et al. (2012). Stability of the Atlantic meridional overturning circulation: A model intercomparison. *Geophysical Research Letters*, *39*, 113. https://doi.org/10.1029/2012GL053763

Weber, T. S., & Deutsch, C. (2010). Ocean nutrient ratios governed by plankton biogeography. *Nature*, *467*(7315), 550–554. https://doi.org/10.1038/nature09403

Wyrwoll, K. H., Dong, B., & Valdes, P. (2000). On the position of southern hemisphere westerlies at the Last Glacial Maximum: An outline of AGCM simulation results and evaluation of their implications. *Quaternary Science Reviews*, *19*(9), 881–898. https://doi.org/10.1016/S0277-3791(99)00047-5

Zickfeld, K., Eby, M., Weaver, A. J., Alexander, K., Crespin, E., Edwards, N. R., et al. (2013). Long-term climate change commitment and reversibility: An EMIC intercomparison. *Journal of Climate*, *26*(16), 5782–5809. https://doi.org/10.1175/JCLI-D-12-00584.1